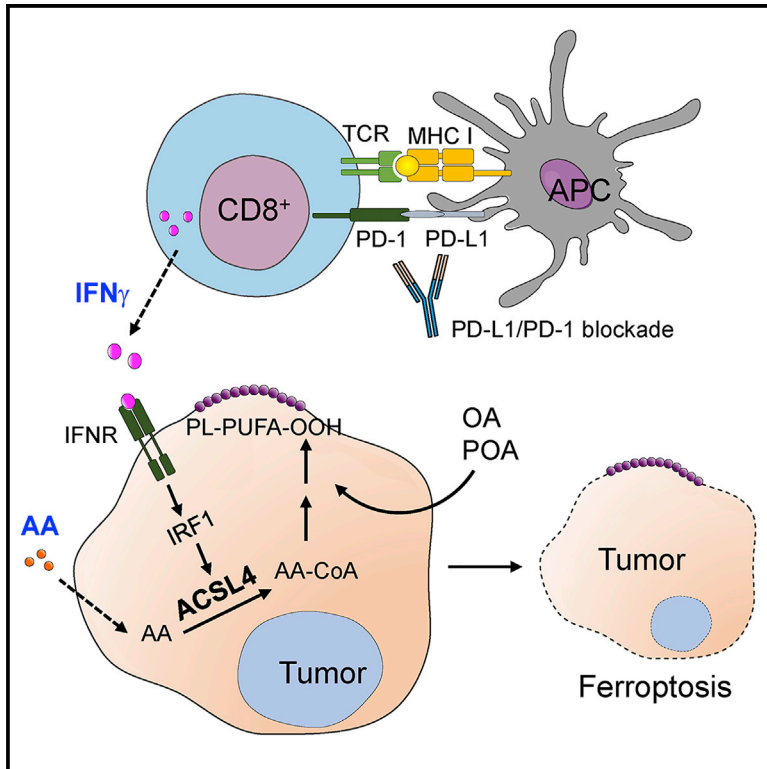# Cancer Cell

CD8+ T cells and fatty acids orchestrate tumor ferroptosis and immunity via ACSL4

Graphical abstract

Authors

Peng Liao, Weimin Wang,
Weichao Wang, ..., Miguel Gijón,
Yatrik M. Shah, Weiping Zou

Correspondence

wzou@med.umich.edu

In brief

In brief: Liao et al. demonstrate IFNγ from cytotoxic T lymphocytes (CTLs) and arachidonic acid from the tumor microenvironment naturally induce tumor cell ferroptosis, which is mediated via ACSL4-dependent lipid reprogramming. Targeting the ACSL4 pathway is a potential anti-cancer approach.

Highlights

- Arachidonic acid and IFNγ coordinately induce tumor cell ferroptosis via ACSL4

- ACSL4-dependent tumor ferroptosis is a mode of action of CTLs

- ACSL4 mediates immunogenic tumor ferroptosis

- Targeting tumor ACSL4 sensitizes checkpoint therapy

CellPress

Cancer Cell

Article

CD8+ T cells and fatty acids orchestrate tumor ferroptosis and immunity via ACSL4

Peng Liao,[1,2,8] Weimin Wang,[1,2,8] Weichao Wang,[1,2] Ilona Kryczek,[1,2] Xiong Li,[1,2] Yingjie Bian,[1,2] Amanda Sell,[1,2] Shuang Wei,[1,2] Sara Grove,[1,2] Jeffrey K. Johnson,[3] Paul D. Kennedy,[3] Miguel Gijón,[3] Yatrik M. Shah,[4] and Weiping Zou[1,2,5,6,7,9,*]

[1]Department of Surgery, University of Michigan School of Medicine, BSRB, 109 Zina Pitcher Place, Ann Arbor, MI, USA
[2]Center of Excellence for Cancer Immunology and Immunotherapy, Rogel Cancer Center, University of Michigan School of Medicine, Ann Arbor, MI, USA
[3]Cayman Chemical Company, Ann Arbor, MI, USA
[4]Department of Molecular and Integrative Physiology, University of Michigan School of Medicine, Ann Arbor, MI, USA
[5]Department of Pathology, University of Michigan School of Medicine, Ann Arbor, MI, USA
[6]Graduate Program in Immunology, University of Michigan School of Medicine, Ann Arbor, MI, USA
[7]Graduate Program in Tumor Biology, University of Michigan School of Medicine, Ann Arbor, MI, USA
[8]These authors contributed equally
[9]Lead contact
*Correspondence: wzou@med.umich.edu
https://doi.org/10.1016/j.ccell.2022.02.003

SUMMARY

Tumor cell intrinsic ferroptosis-initiating mechanisms are unknown. Here, we discover that T cell-derived interferon (IFN)γ in combination with arachidonic acid (AA) induces immunogenic tumor ferroptosis, serving as a mode of action for CD8+ T cell (CTL)-mediated tumor killing. Mechanistically, IFNγ stimulates ACSL4 and alters tumor cell lipid pattern, thereby increasing incorporations of AA into C16 and C18 acyl chain-containing phospholipids. Palmitoleic acid and oleic acid, two common C16 and C18 fatty acids in blood, promote ACSL4-dependent tumor ferroptosis induced by IFNγ plus AA. Moreover, tumor ACSL4 deficiency accelerates tumor progression. Low-dose AA enhances tumor ferroptosis and elevates spontaneous and immune checkpoint blockade (ICB)-induced anti-tumor immunity. Clinically, tumor ACSL4 correlates with T cell signatures and improved survival in ICB-treated cancer patients. Thus, IFNγ signaling paired with selective fatty acids is a natural tumor ferroptosis-promoting mechanism and a mode of action of CTLs. Targeting the ACSL4 pathway is a potential anti-cancer approach.

INTRODUCTION

Ferroptosis was discovered by studying the cytotoxic effects of small synthetic molecules, such as erastin and RSL3, in cultured tumor cells *in vitro* (Dixon and Stockwell, 2019). These small molecules artificially induce ferroptosis by targeting cystine uptake, glutathione (GSH) synthesis, iron loading, glutathione peroxidase-4 (GPX4) activity, and ferroptosis suppressor protein-1 (FSP1) (Doll et al., 2019) (Bersuker et al., 2019). Interestingly, accumulating evidence indicates that ferroptosis may be implicated in a variety of pathological scenarios, including acute kidney injury, tissue ischemia and reperfusion injury, neurodegeneration, and cancer. However, natural ferroptosis-inducing mechanisms in these conditions remain unknown.

Immune checkpoint blockade (ICB)-activated CD8+ T cells in the tumor microenvironment can sensitize tumor cell ferroptosis. The combination of a synthetic ferroptosis inducer and programmed death ligand 1 (PD-L1) blockade synergistically enhances the anti-tumor efficacy in preclinical models (Lang et al., 2019; Wang et al., 2019). Moreover, T cell-derived IFNγ

sensitizes tumor cell ferroptosis induced by erastin or RSL3 in the *in vitro* culture system (Wang et al., 2019). However, IFNγ alone failed to directly initiate and induce tumor cell ferroptosis *in vitro* (Wang et al., 2019). Whether and how tumor cells can undergo endogenous ferroptosis in the absence of synthetic chemical inducers remains elusive. Ferroptosis is regulated by fatty acid metabolism (Kagan et al., 2017) (Hassannia et al., 2019; Magtanong et al., 2019). Fatty acids consist of short-chain fatty acids (SCFA), medium-chain fatty acids (MCFA), long-chain fatty acids (LCFA), and very-long-chain fatty acids (VLCFA). Moreover, fatty acids include saturated and unsaturated (monounsaturated and polyunsaturated) species. Here, we have screened and tested the ferroptotic potential of different fatty acids in combination with IFNγ on *in vitro* cultured tumor cells. We have also enlisted a multidisciplinary approach utilizing targeted lipidomics analysis and multiple tumor models to explore the cross talk between the immune system (such as CD8+ T cells and IFNγ) and lipid metabolism (such as different fatty acids) in the context of tumor ferroptosis in the tumor microenvironment and its relevance in cancer immunity and therapy.
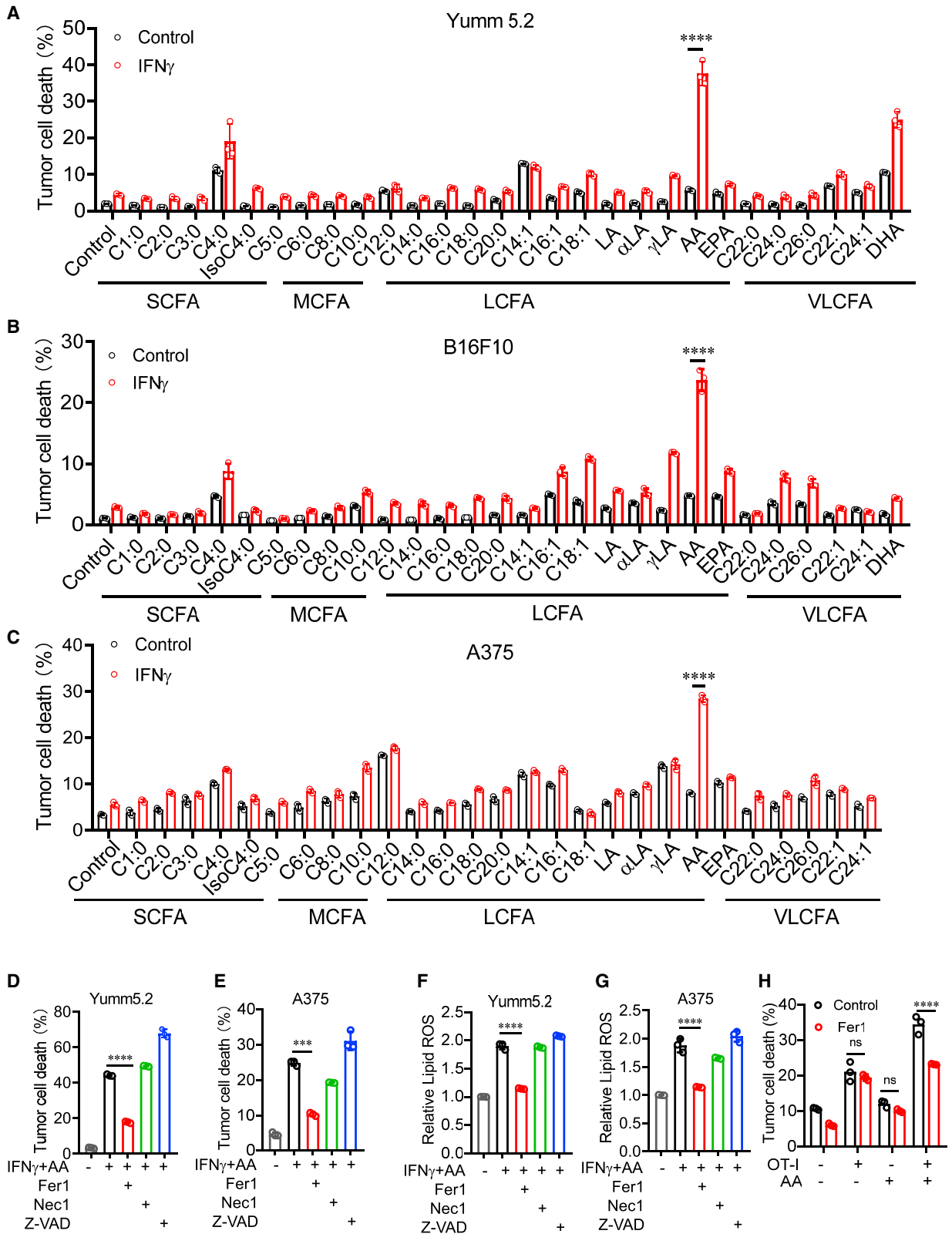
(legend on next page)

RESULTS

Arachidonic acid and IFNγ coordinately induce tumor cell ferroptosis

We hypothesized that IFNγ could cooperate with selective fatty acids to induce tumor cell ferroptosis without synthetic inducers. To test this hypothesis, we screened and tested ferroptotic potential of all typical fatty acids (Table S1) in inducing both mouse and human tumor cell death with or without IFNγ (Psychogios et al., 2011). As expected, IFNγ or individual fatty acids alone failed to induce cell death in two murine melanoma lines, Yumm5.2 and B16F10, and a human melanoma line, A375 (Figures 1A–1C). Interestingly, arachidonic acid, but not other fatty acids, synergized with IFNγ to induce potent cell death in all three tumor cell lines (Figures 1A–1C). Thereafter, we focused our studies on arachidonic acid. Physiological levels of arachidonic acid are approximately 13 μM in peripheral blood (Zabielski et al., 2014). We treated Yumm5.2 cells with IFNγ in the presence of different concentrations of arachidonic acid, starting with 10 μM. We found that arachidonic acid promoted tumor lipid reactive oxygen species (ROS) production and cell death in a dose- (Figures S1A–S1B) and time- (Figures S1C and S1D) dependent manner.

To determine whether the combination of IFNγ and arachidonic acid induces tumor cell death via ferroptosis, we treated Yumm5.2 cells and A375 cells with IFNγ and arachidonic acid in the presence of different cell death inhibitors, including ferrostatin-1 (Fer1), a specific ferroptosis inhibitor; necrostatin-1 (Nec1), a necrosis inhibitor; and Z-VAD-fmk (Z-VAD), an apoptosis inhibitor. The combination of IFNγ and arachidonic acid induced Yumm5.2 and A375 cell death, and Fer1, but not other inhibitors, rescued both Yumm5.2 and A375 cell death (Figures 1D and 1E). Furthermore, the combination of IFNγ and arachidonic acid increased lipid ROS in Yumm5.2 (Figure 1F) and A375 (Figure 1G) cells, which was also reversed by Fer1 (Figures 1F and 1G). Thus, the combination of IFNγ and arachidonic acid causes tumor cell death via inducing tumor ferroptosis in the absence of synthetic ferroptosis inducer. Tumor antigen-specific CD8$^+$ T cells promote tumor cell ferroptosis via IFNγ (Wang et al., 2019). We tested whether arachidonic acid altered tumor killing mediated by antigen-specific CD8$^+$ T cells. We cultured ovalbumin-expressing (OVA$^+$)-Yumm5.2 cells with OVA-specific CD8$^+$ T (OT-I) cells in the presence of arachidonic acid. We observed that supplementation of arachidonic acid increased OT-I-mediated tumor cell death, which could be rescued by Fer1 (Figure 1H). Thus, arachidonic acid and CD8$^+$ T cells (or IFNγ) can coordinately induce tumor cell ferroptosis.

Arachidonic acid and IFNγ induce tumor cell ferroptosis via ACSL4

We next explored the mechanism by which IFNγ plus arachidonic acid induce tumor cell ferroptosis. Acyl-CoA synthetase long-chain family member 4 (ACSL4) activates arachidonic acid to arachidonyl-CoA, which is esterified into phospholipids. Exogenous arachidonic acid enhances RSL3-induced ferroptosis (Doll et al., 2017). In line with a previous report (Kagan et al., 2017), arachidonic acid alone failed to directly trigger tumor cell ferroptosis (Figures 1A–1C). We questioned whether ACSL4 is a critical enzyme for arachidonic acid plus IFNγ to induce tumor cell ferroptosis. We generated Acsl4-deficient (Acsl4$^{-/-}$) Yumm5.2 cells (Figure 2A). As expected, Acsl4$^{-/-}$ Yumm5.2 cells were resistant to RSL3, a synthetic ferroptosis inducer, compared with wild-type (Acsl4$^{+/+}$) cells (Figure 2B). Acsl4 deficiency abolished Yumm5.2 tumor cell death (Figure 2C) and lipid ROS production (Figure 2D) induced by the combination of IFNγ and arachidonic acid. In addition, we treated Yumm5.2 cells with rosiglitazone, an enzymatic inhibitor of ACSL4 (Kim et al., 2001). We found that rosiglitazone prevented Yumm5.2 tumor cell death induced by IFNγ and arachidonic acid in a dose-dependent manner (Figure S2A). We extended our study to MC38 colon tumor cells. Similarly, Acsl4$^{-/-}$ MC38 cells were resistant to ferroptosis induced by RSL3 (Figure 2E) and the combination of IFNγ plus arachidonic acid (Figure 2F) compared with Acsl4$^{+/+}$ MC38 cells. Furthermore, in the co-culture of OVA$^+$-Yumm5.2 cells and OT-I cells, supplementation of arachidonic acid enhanced Acsl4$^{+/+}$ tumor cell death but not Acsl4$^{-/-}$ tumor cell death (Figure 2G). To demonstrate tumor incorporation of arachidonic acid, we detected intracellular arachidonic acid in tumor cells when exogeneous arachidonic acid was provided in the in vitro culture (Figure S2B). We next performed an Acsl4 rescue experiment. Considering that constitutively forced ACSL4 expression might directly affect tumor cell death, we used a doxycycline (Dox)-inducible system to mediate ACSL4 re-expression in Acsl4$^{-/-}$ Yumm5.2 cells (Figure 2H). We observed that forced ACSL4 expression sensitized tumor cell death induced by OT-I cells in the presence of arachidonic acid (Figure 2I) and by the combination of IFNγ plus arachidonic acid (Figure 2J). Furthermore, supplementation of arachidonic acid enhanced tumor cell killing (Figure 2K) and lipid ROS production (Figure 2L) induced by activated CD8$^+$ T-cells. These effects were abolished by anti-IFNγ monoclonal antibody (mAb) but not by anti-TNFα mAb (Figures 2K and 2L). Arachidonic acid can be obtained from diet or from the essential fatty acid linoleic acid by desaturation and chain elongation. We detected arachidonic acid in peripheral blood and tumor tissues in Yumm5.2 tumor-bearing mice (Figure 2M). IFNγ is often produced by activated T cells and

---

Figure 1. Arachidonic acid (AA) and IFNγ coordinately induce tumor cell ferroptosis

(A–C) Percentage of dead Yumm5.2 (A), B16F10 (B), and A375 (C) cells that were treated with IFNγ and common fatty acids for 3 days (n = 3). See also Table S1.

(D and E) Percentage of dead Yumm5.2 (D) and A375 (E) cells treated with IFNγ and AA in the presence of ferrostatin-1 (Fer1, 2 μM), necrostatin-1 (Nec1, 1 μM), or z-VAD-FMK (z-VAD, 10 μM) for 3 days; 10 (D) and 50 (E) ng/mL IFNγ, and 20 (D) and 30 (E) μM AA (n = 3).

(F and G) Lipid ROS in Yumm5.2 (F) and A375 (G) cells treated with IFNγ and AA in the presence of ferrostatin-1 (Fer1, 2 μM) for 3 days, 10 (F) and 50 (G) ng/mL IFNγ, and 20 (F) and 30 (G) μM AA (n = 3).

(H) Percentage of dead OVA-pulsed Yumm5.2 cells in co-cultures with OT-I cells (tumor: OT-I ratio of 1:2) in the presence of AA (20 μM) and (Fer1; 2 μM) for 48 h (n = 3). Data are shown as mean ± SD, two-way ANOVA(A–C and H) or one-way ANOVA(D–G). ***p < 0.001, ****p < 0.0001; ns, not significant.
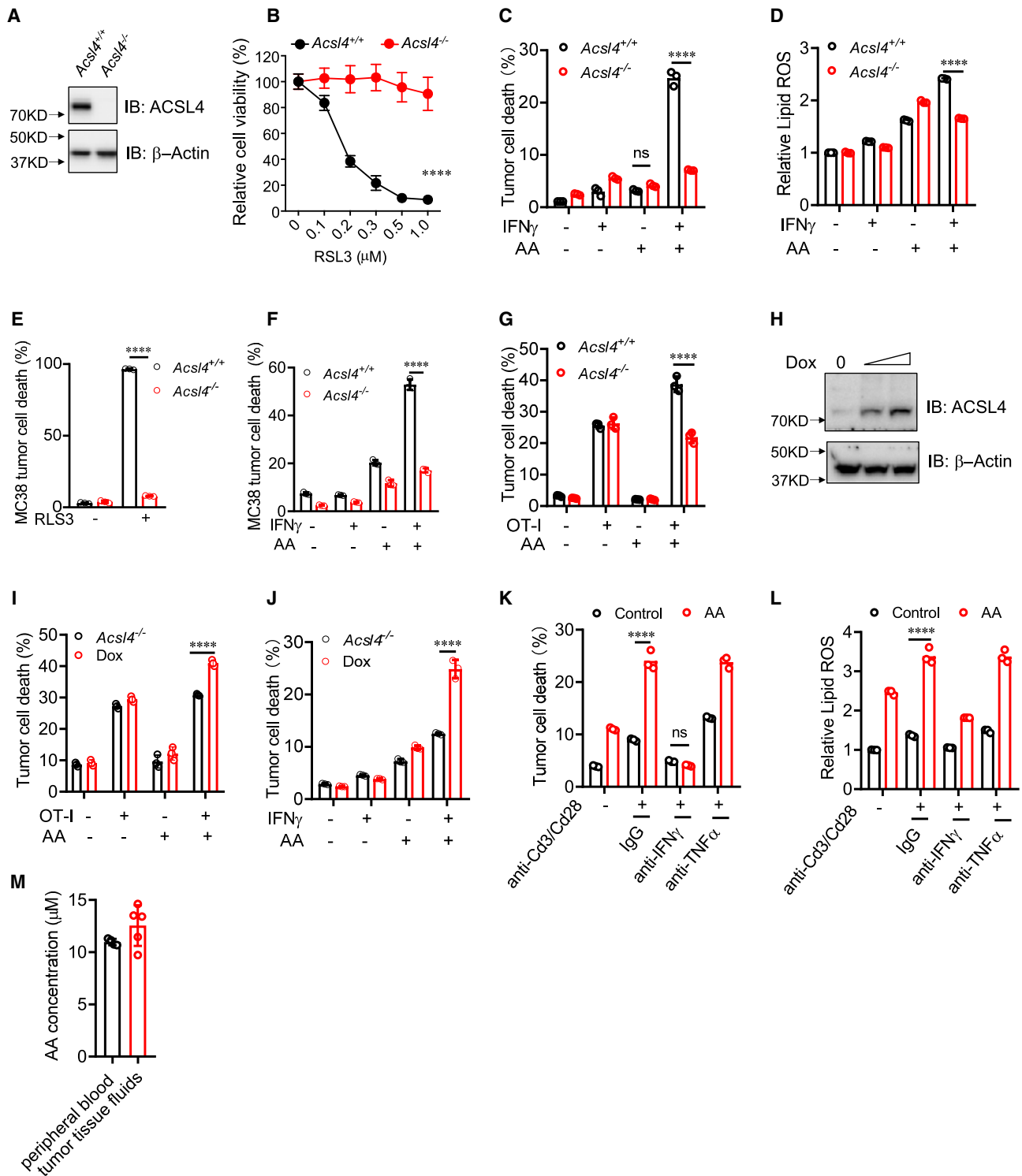
See also Figure S1 and Table S1.

Figure 2. AA and IFNγ induce tumor cell ferroptosis via ACSL4

(A) Immunoblots of ACSL4 in $Acsl4^{+/+}$ or $Acsl4^{-/-}$ Yumm5.2 cells.

(B) Relative cell viability of $Acsl4^{+/+}$ or $Acsl4^{-/-}$ Yumm5.2 cells treated with different concentrations of RSL3 for 24 h (n = 3).

(C and D) Percentage of dead cells (C) or relative lipid ROS (D) in $Acsl4^{+/+}$ or $Acsl4^{-/-}$ Yumm5.2 cells treated with IFNγ and AA for 3 days (n = 3).

(E) Percentage of dead $Acsl4^{+/+}$ or $Acsl4^{-/-}$ MC38 cells treated with RSL3 for 24 h (n = 3).

(F) Percentage of dead $Acsl4^{+/+}$ or $Acsl4^{-/-}$ MC38 cells treated with IFNγ and AA for 3 days (n = 3).

(G) Percentage of dead OVA⁺ $Acsl4^{+/+}$ or $Acsl4^{-/-}$ Yumm5.2 cells cultured with OT-I cells (tumor: OT-I ratio of 1:2) in the presence of AA for 48 h (n = 3).

NK cells. Hence, the simultaneous presence of arachidonic acid and IFNγ could be a natural condition and mechanism capable of inducing tumor cell ferroptosis in the tumor microenvironment.

Given that system X_c^- and IFNγ regulate cell ferroptosis (Dixon and Stockwell, 2019; Wang et al., 2019), we wondered if system X_c^- was involved in tumor ferroptosis induced by IFNγ plus arachidonic acid. To this end, we examined Yumm5.2 cell ferroptosis induced by erastin or IFNγ plus arachidonic acid in the presence of cysteine. Erastin inhibited system X_c^-, leading to cystine starvation, glutathione depletion, and consequently ferroptotic cell death. As expected, addition of cysteine bypassed system X_c^- and blocked erastin-induced tumor ferroptosis (Figure S2C). However, addition of cysteine failed to alter tumor ferroptosis induced by IFNγ plus arachidonic acid (Figure S2D). These results provide additional evidence that ACSL4, not system X_c^-, is critical for tumor ferroptosis induced by IFNγ plus arachidonic acid. All together, our results reveal that activated T cell-derived IFNγ paired with arachidonic acid in the tumor microenvironment can induce tumor cell ferroptosis via ACSL4.

IFNγ stimulates ACSL4 expression via STAT1 and IRF1 signaling

Given the necessity of ACSL4 in tumor ferroptosis induced by the combination of arachidonic acid and IFNγ, we hypothesized that IFNγ regulates ACSL4 expression in tumor cells. To test this hypothesis, we cultured Yumm5.2 cells with IFNγ at different time points. IFNγ treatment enhanced *Acsl4* expression in Yumm5.2 and MC38 cells at both mRNA and protein levels (Figures 3A–3D). As positive controls, IFNγ treatment stimulated expression of IFNγ-responsive genes, such as interferon regulatory factor 1 (IRF1) (Figure 3E). IFNγ signaling regulates gene expression through the Janus kinase (JAK)-signal transducer and activator of transcription 1 (STAT1) pathway. Using CRISPR-Cas9 technology, we established *Stat1*-deficient (*Stat1*$^{-/-}$) Yumm5.2 cells. As expected, IFNγ treatment failed to stimulate *Stat1* transcript (Figure 3F), and STAT1 and IRF1 protein expression (Figure 3G) in *Stat1*$^{-/-}$ Yumm5.2 cells compared with wild-type cells. IFNγ treatment failed to facilitate *Acsl4* expression in *Stat1*$^{-/-}$ Yumm5.2 cells compared with wild-type cells at both mRNA and protein levels (Figures 3H and 3I). Interestingly, IFNγ plus arachidonic acid failed to induce *Stat1*$^{-/-}$ tumor cell ferroptosis (Figure 3J) and lipid ROS production (Figure 3K) compared with wild-type cells. Upon JAK/STAT1 activation via IFNγ, IRF1 binds to IFN-stimulated response element (ISRE), thereby initiating the transcription of IFNγ-responsive genes. The ENCODE chromatin immunoprecipitation (ChIP)-seq database suggests the exis-

tence of the binding sites for IRF1 at the promotor region of *ACSL4* but not for STAT1 (Figure 3L) (Consortium, 2012). Further analysis revealed five potential IRF1 binding sites (BS1-5) in the promoter region of *ACSL4* (Figure 3L). ChIP assay identified BS2 and BS3 as the major IRF1 binding sites in the putative promoter of *ACSL4* in A375 cells (Figure 3M). All together, these results suggest that *ACSL4* is a previously unknown IFNγ-responsive gene and that STAT1 activation is essential for *ACSL4* expression and tumor cell ferroptosis induced by arachidonic acid plus IFNγ.

IFNγ reprograms ACSL4 associated phospholipids to induce tumor ferroptosis

Cellular lipid composition and fatty acid metabolism control ferroptosis (Dixon and Stockwell, 2019; Kraft et al., 2020; Zou et al., 2020). Apart from ACSL4 expression, we wondered if IFNγ in combination with arachidonic acid altered tumor cell lipids. Interestingly, targeted phospholipid analysis in *Acsl4*$^{+/+}$ and *Acsl4*$^{-/-}$ Yumm5.2 cells treated with IFNγ, deuterated arachidonic acid-d_5 (AA-d_5), and their combination demonstrated distinct lipid clusters in different experimental conditions (Figure S3A). Arachidonic acid or IFNγ slightly changed the relative abundance of different phospholipid species in *Acsl4*$^{+/+}$ Yumm5.2 cells (Figure 4A). Treatment with arachidonic acid-d_5 plus IFNγ increased the total arachidonic acid-associated phospholipid species in *Acsl4*$^{+/+}$ Yumm5.2 cells compared with *Acsl4*$^{-/-}$ Yumm5.2 cells (Figure S3B). Interestingly, when we compared the impact of arachidonic acid-d_5 on different phospholipid species, we found that arachidonic acid was preferentially integrated into C16 and C18 acyl chain-containing phospholipids in an ACSL4-dependent manner (Figure S3C). Arachidonic acid-d_5 was preferentially integrated into phosphatidylethanolamine (PE) and phosphatidylcholine (PC) species, particularly in C16:0, C16:1, C18:0, and C18:1 species (Figures 4B and 4C). This effect was amplified by IFNγ (Figures 4B and 4C). Taken together, the data indicate that IFNγ alters ACSL4 expression and lipids to induce tumor ferroptosis.

Given that arachidonic acid-d_5 was preferentially integrated into C16 and C18 acyl chain-containing phospholipids and IFNγ synergized with this integration, we posit that certain C16 and C18 fatty acids could participate in tumor ferroptosis induced by the combination of IFNγ and arachidonic acid. To explore this possibility, we turned our attention to the common C16 and C18 fatty acids in human peripheral blood. Blood C16 fatty acids include 16:0 (palmitic acid, PA) and 16:1. C16:1 isomers consist mainly of palmitoleic acid (POA), palmitelaidic acid (PEA), and sapienic acid (SAA) (Psychogios et al., 2011; Sommerfeld, 1983) (Table S2). To test a potential role of common

---

(H) Immunoblots of Acsl4 in inducible Acsl4 expression in *Acsl4*$^{-/-}$ Yumm5.2 cells transfected with Tet-On-inducible ACSL4 expression plasmids. Cells were treated with or without Dox (0.2 or 0.5 μg/mL).

(I) Percentage of dead OVA$^+$ in *Acsl4*$^{-/-}$ Yumm5.2 cells cultured with OT-I cells in the presence of AA for 48 h. Yumm5.2 cells were pretreated with or without Dox (0.2 μg/mL) for 2 days to induce ACSL4 expression (n = 3).

(J) Percentage of dead Yumm5.2 cells treated with IFNγ and AA for 3 days. Yumm5.2 cells were pretreated with or without Dox (1 μg/mL) for 2 days to induce Acsl4 expression (n = 3).

(K and L) Percentage of dead cells (K) or relative lipid ROS (L) in *Acsl4*$^{+/+}$ or *Acsl4*$^{-/-}$ Yumm5.2 cells treated with supernatant from activated CD8$^+$ T cells in the presence of anti-IFNγ or anti-TNFα blocking mAbs for 3 days (n = 3).

(M) AA levels in peripheral blood or Yumm5.2 tumor tissues of tumor-bearing mice measured by ELISA (n = 4–5). Data are shown as mean ± SD, two-way ANOVA(B–G and I–L). ****p < 0.0001; ns, significant. Immunoblots, one of three experiments is shown.
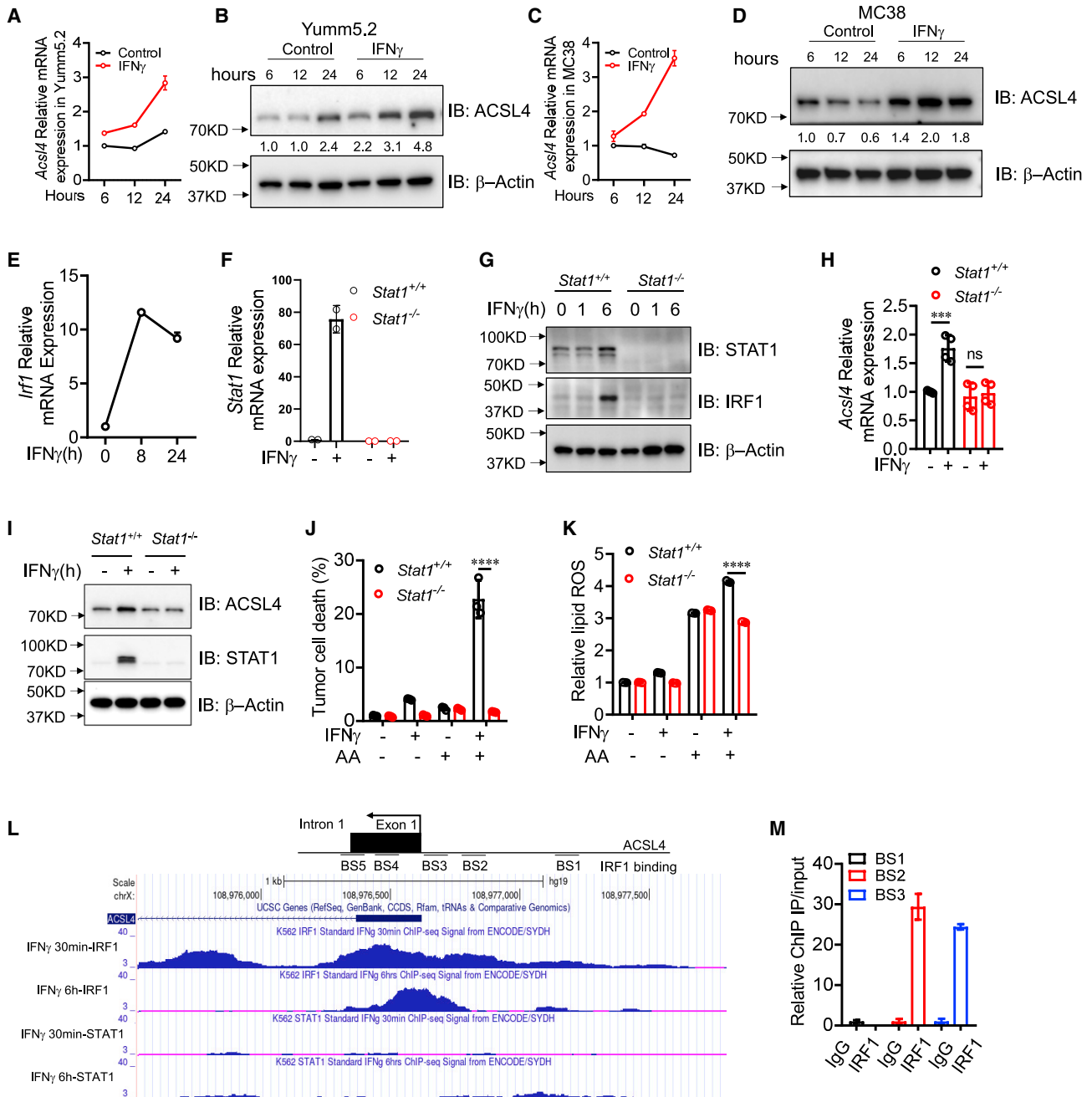
See also Figure S2.

Figure 3. IFNγ stimulates ACSL4 expression via STAT1 and IRF1 signaling

(A and B) *Acsl4* transcripts (A) and proteins (B) in Yumm5.2 cells treated with IFNγ at indicated times (n = 2–3)

(C and D) *Acsl4* transcripts (C) and proteins (D) in MC38 cells treated with IFNγ at different times (n = 2–3).

(E) *Irf1* transcripts in Yumm5.2 cells treated with IFNγ at different times (n = 2).

(F) *Stat1* transcripts in *Stat1*$^{+/+}$ or *Stat1*$^{-/-}$ Yumm5.2 cells treated with IFNγ for 24 h (n = 2).

(G) Immunoblots of STAT1 and IRF1 in *Stat1*$^{+/+}$ or *Stat1*$^{-/-}$ Yumm5.2 cells treated with IFNγ at different times.

(H and I) *Acsl4* transcripts (H) and proteins (I) in *Stat1*$^{+/+}$ or *Stat1*$^{-/-}$ Yumm5.2 cells treated with IFNγ for 24 h (n = 3–4).

(J and K) Percentage of dead cells (J) and relative lipid ROS (K) in *Stat1*$^{+/+}$ or *Stat1*$^{-/-}$ Yumm5.2 cells treated with IFNγ and AA for 3 days (n = 3).

(L) IRF1 ChIP-seq data from ENCODE shows the IRF1 binding sites at the ACSL4 promoter region.

(M) ChIP of IRF1 in A375 cells treated with or without IFNγ. IRF1 binding to ACSL4 TSS region was quantified by qPCR. Results are expressed as fold change in the specific site occupancy over control (n = 2). Data are shown as mean ± SD, two-way ANOVA(H, J, and K). ***p < 0.001, ****p < 0.0001; ns, not significant. Immunoblots, one of three experiments is shown.
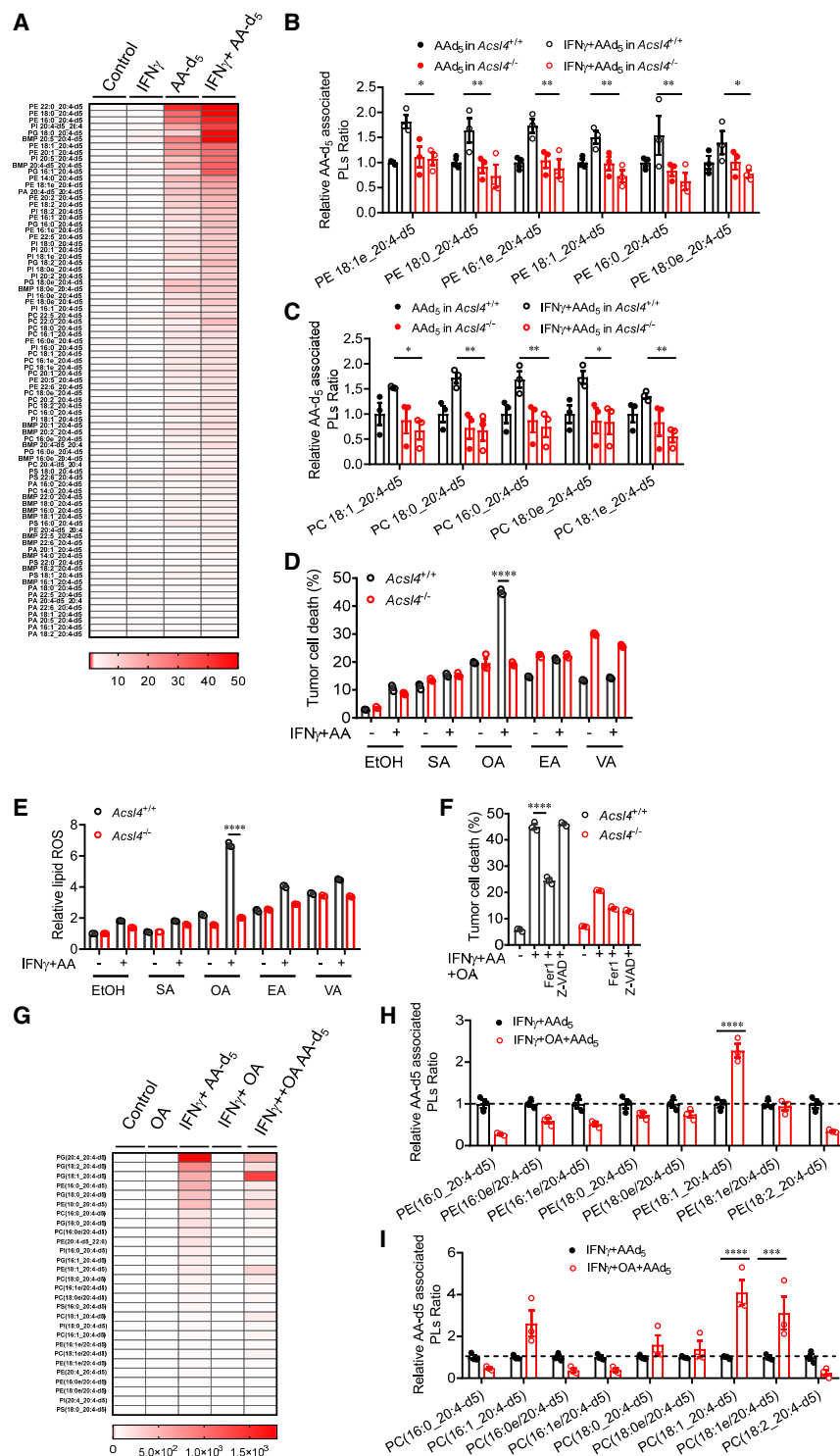
Figure 4. IFNγ reprograms ACSL4-associated phospholipids to induce tumor ferroptosis

(A–C) Effect of IFNγ plus AA-d5 on tumor phospholipids. Yumm5.2 cells treated with IFNγ (10 ng/mL), AA-d5 (10 μM), and their combination for 48 h. Lipids were analyzed by ultra-performance liquid chromatography-tandem mass spectrometry (UPLC-MS/MS). Heatmap shows phospholipid fold-changes in Yumm5.2 cells (A). Phosphatidylethanolamine (PE), phosphatidylcholine (PC), phosphatidylglycerol (PG), phosphatidylserine (PS), phosphatidylinositol (PI), phosphatidic acid (PA), and Bis (monoacylglycero)phosphate (BMP); "e" represents ether phospholipid. The relative changes of different phospholipids (A), PE (B), and PC (C) that contain C16 and C18 acyl chain are shown (n = 3).

(D and E) Percentage of dead cells (D) or relative lipid ROS (E) in $Acsl4^{+/+}$ or $Acsl4^{-/-}$ Yumm5.2 cells treated with IFNγ and low-dose AA (10 μM) for 48 h in the presence of stearic acid (SA, 20 μM), oleic acid (OA, 60 μM), elaidic acid (EA, 60 μM), and *trans*-vaccenic acid (VA, 60 μM) (n = 3).

(F) Percentage of dead cells in $Acsl4^{+/+}$ or $Acsl4^{-/-}$ Yumm5.2 cells treated with IFNγ, AA (10 μM), and OA (60 μM) in the presence of Fer1 or z-VAD for 48 h (n = 3).

(G–I) Effect of IFNγ plus AA-d5 and OA on tumor phospholipids. Yumm5.2 cells treated with OA (60 μM), IFNγ (10 ng/mL) + AA-d5 (10 μM), IFNγ + OA or their combination for 48 h. Lipids were analyzed by UPLS-MS/MS. Heatmap shows phospholipid fold changes in Yumm5.2 cells (G). The relative changes of different phospholipids (G), and PE (H), and PC (I) of C16 and C18 acyl chain-containing phospholipids are shown in Yumm5.2 cells (n = 3). Data are shown as mean ± SEM(A–C and G–I), mean ± SD(D–F), two-way ANOVA(B–F, H and L). $*p < 0.05$, $**p < 0.01$, $***p < 0.001$, and $****p < 0.0001$.
See also Figure S3 and Table S2.

$Acsl4^{+/+}$ Yumm5.2 cells but not in $Acsl4^{-/-}$ Yumm5.2 cells (Figure S3E). In addition, Fer1, but not Z-VAD, abolished the effect of POA on $Acsl4^{+/+}$ Yumm5.2 cell death (Figure S3E). Common C18:0 and C18:1 fatty acids in peripheral blood include C18:0 (stearic acid, SA) and C18:1 isomers, which mainly consist of oleic acid (OA), elaidic acid (EA), and vaccenic acid (VA) (Psychogios et al., 2011; Sommerfeld, 1983) (Table S2). We performed similar experiments to test a potential role of common C18 fatty acids in

C16 fatty acids in tumor cell ferroptosis, we cultured $Acsl4^{+/+}$ and $Acsl4^{-/-}$ Yumm5.2 cells with these fatty acids in the presence of IFNγ and low-dose arachidonic acid. We observed that POA, but not other C16-fatty acids, enhanced tumor cell lipid ROS production in $Acsl4^{+/+}$ tumor cells compared with $Acsl4^{-/-}$ tumor cells (Figure S3D). As expected, POA induced cell death in

tumor cell ferroptosis. We found that OA, but not other C18 fatty acids, enhanced tumor cell death (Figure 4D) and lipid ROS production (Figure 4E) in $Acsl4^{+/+}$ tumor cells compared with $Acsl4^{-/-}$ tumor cells. Furthermore, the effect of OA on tumor cell death was reversed by Fer1, but not by Z-VAD (Figure 4F). The data indicate that OA promotes tumor cell ferroptosis

initiated by IFNγ plus arachidonic acid. However, it has been reported (Magtanong et al., 2019; Yang et al., 2016b), and we confirmed, that OA inhibited erastin-induced ferroptosis in vitro (Figure S3F). The results suggest a context-dependent role of OA in tumor cell ferroptosis. To further determine this possibility, we examined whether OA or OA plus IFNγ could induce tumor cell ferroptosis in the absence of arachidonic acid. We found that OA or OA plus IFNγ had no obvious effect on Yumm5.2 cell death (Figure S3G). Then, we performed a target lipidomic assay in Yumm5.2 cells treated with IFNγ plus arachidonic acid-d5 in the presence or absence of OA. The PCA analysis demonstrated distinct lipid clusters in different conditions (Figure S3H). We tracked how OA affected the composition of arachidonic acid acyl chain-containing phospholipids, specifically analyzing arachidonic acid-d5-incorporated phospholipids (Figure 4G). We found that OA resulted in an increase in 18:1_20:4-d$_5$ phospholipids in the major lipid species of PE (Figure 4H) and PC (Figure 4I). The data suggest that IFNγ reprograms ACSL4-associated phospholipids to induce tumor ferroptosis, and the common C16 and C18 fatty acids, such as POA and OA, can participate in this process.

Tumor ACSL4 affects anti-tumor immunity

The combination of arachidonic acid and IFNγ is an endogenous trigger for tumor cell ferroptosis via ACSL4. This mechanism may participate in CD8$^+$ T cell-mediated tumor killing. As $Acsl4^{-/-}$ tumor cells are relatively resistant to ferroptotic cell death compared with $Acsl4^{+/+}$ tumor cells, we hypothesized that $Acsl4^{-/-}$ and $Acsl4^{+/+}$ tumor cells manifested different T cell responses in vivo due to their differences in ferroptotic death and potential tumor antigen release and spread. To test this hypothesis, we inoculated $Acsl4^{-/-}$ and $Acsl4^{+/+}$ Yumm5.2 cells into NOD.SCID γc-deficient (NSG) (immune-deficient) mice and C57BL/6J (immunocompetent) mice. $Acsl4^{-/-}$ and $Acsl4^{+/+}$ Yumm5.2 tumors comparably progressed in NSG mice (Figure 5A), were similarly proliferative in vitro (Figure S4A), and equally sensitive to cisplatin-induced apoptosis (Figure S4B). However, $Acsl4^{-/-}$ tumors grew faster and larger in C57BL/6J (immunocompetent) mice as shown by tumor volume (Figure 5B) and tumor weight (Figure 5C) compared with $Acsl4^{+/+}$ tumors. $Acsl4^{-/-}$ tumors expressed lower levels of lipid ROS than $Acsl4^{+/+}$ tumors in vivo (Figure 5D). Mice bearing $Acsl4^{-/-}$ tumors experienced a shorter survival than their counterparts (Figure 5E), and harbored reduced amounts of CD8$^+$ and CD4$^+$ T cells (Figures 5F, 5G, and S4C), and IFNγ$^+$ and TNFα$^+$CD8$^+$ and CD4$^+$ T cells in the tumor microenvironment (Figures 5H–5K). We extended our studies to the MC38 colon tumor model. We inoculated $Acsl4^{-/-}$ and $Acsl4^{+/+}$ MC38 cells in NSG (Figure 5L) and C57/BL6 mice (Figure 5M). As in the Yumm5.2 tumor model, $Acsl4^{-/-}$ and $Acsl4^{+/+}$ MC38 tumors grew similarly in NSG mice (Figure 5L), but $Acsl4^{-/-}$ MC38 tumors rapidly progressed in the immunocompetent C57BL/6J mice compared with $Acsl4^{+/+}$ MC38 tumors, as shown by tumor volume (Figure 5M) and tumor weight (Figure 5N). Again, $Acsl4^{-/-}$ MC38 tumors harbored lower amounts of CD8$^+$ and CD4$^+$ T cells (Figures 5O and 5P) and IFNγ$^+$CD8$^+$ and CD4$^+$ T cells (Figures 3Q and 3R) compared with $Acsl4^{+/+}$ MC38 tumors. We additionally generated $Acsl4^{-/-}$ B16F10 cells. $Acsl4^{-/-}$ B16F10 cells were resistant to RSL3-induced cell death (Figure S4D) but were sensitive

to cisplatin-induced apoptosis (Figure S4E). $Acsl4^{+/+}$ and $Acsl4^{-/-}$ B16F10 cells had similar proliferation ability in vitro (Figure S4F). However, $Acsl4^{-/-}$ B16F10 tumors rapidly progressed in C57BL/6J mice compared with $Acsl4^{+/+}$ B16F10 tumors (Figure 5S), and harbored lower amounts of CD8$^+$ T cells (Figure 5T) and IFNγ$^+$CD8$^+$ and CD4$^+$ T cells (Figures 5U and 5V). These results demonstrate that tumor ACSL4 deficiency weakens anti-tumor T cell responses.

To explore whether tumor ACSL4 status differentially and directly altered T cell function, we activated T cells in the presence of $Acsl4^{+/+}$ and $Acsl4^{-/-}$ tumor cells in vitro and detected comparable T cell IL-2 and granzyme B in the two groups (Figures S4G and S4H). In addition, tumor ACSL4 might differentially and indirectly alter T cell function via prostaglandin E2 (PGE2). Indeed, ACSL4 plays a controversial role in PGE2 production in different types of cells (Golej et al., 2011; Kuwata et al., 2019; Reeves et al., 2021). It is well known that PGE2 negatively affects anti-tumor immune responses, and inhibition of cyclooxygenase (COX) 2 can sensitize ICB in tumor bearing animal models (Bottcher et al., 2018; Li et al., 2016; Zelenay et al., 2015). To determine whether PGE2 is critically involved in the different immune responses in the tumor microenvironment in mice bearing $Acsl4^{-/-}$ and $Acsl4^{+/+}$ Yumm5.2 cells, we measured PGE2 in $Acsl4^{-/-}$ and $Acsl4^{+/+}$ Yumm5.2 tumor tissues and detected comparable levels of PGE2 in these two groups (Figure S4I). Taken together, these results suggest that tumor ACSL4 affects spontaneous anti-tumor immunity in vivo via control of tumor ferroptosis.

Targeting tumor ferroptosis sensitizes checkpoint therapy

IFNγ signaling plays a central role in spontaneous and ICB-induced immunity (Ayers et al., 2017; Farrar and Schreiber, 1993). Given that arachidonic acid plus IFNγ induced tumor cell ferroptosis (Figures 1A–1C), we hypothesized that arachidonic acid supplementation as a substrate for ACSL4 might induce tumor cell ferroptosis in vivo, inhibit tumor progression, and synergize the anti-tumor effect of PD-L1 blockade in immunocompetent mice. To test this hypothesis, we treated mice bearing three types of tumors, including MC38, Yumm5.2, and Lewis lung carcinoma (LLC), with low-dose arachidonic acid. These tumors manifest high to low sensitivity to immune checkpoint therapy (Lin et al., 2018). Similar to anti-PD-L1 therapy, arachidonic acid alone slowed down MC38 tumor growth, and the combination of arachidonic acid and anti-PD-L1 yielded additional tumor inhibition (Figure 6A). We conducted similar experiments in Yumm5.2 tumor-bearing mice. Again, treatment with arachidonic acid and anti-PD-L1 comparably reduced tumor growth, and their combination therapy resulted in superior tumor suppression compared with single treatment (Figure 6B). Administration of arachidonic acid led to increased levels of arachidonic acid in tumor tissues (Figure S5A). In line with this, the combination therapy increased the percentages of IFNγ$^+$, TNFα$^+$, and granzyme B$^+$CD8$^+$ T cells in the tumor microenvironment (Figures 6C–6E). Furthermore, we treated mice bearing LLC tumors, a checkpoint therapy-resistant tumor line (Lin et al., 2018). Interestingly, treatment with arachidonic acid also yielded anti-tumor efficacy (Figure 6F), accompanied by an increase in IFNγ$^+$, TNFα$^+$, and granzyme B$^+$CD8$^+$ T cells in the
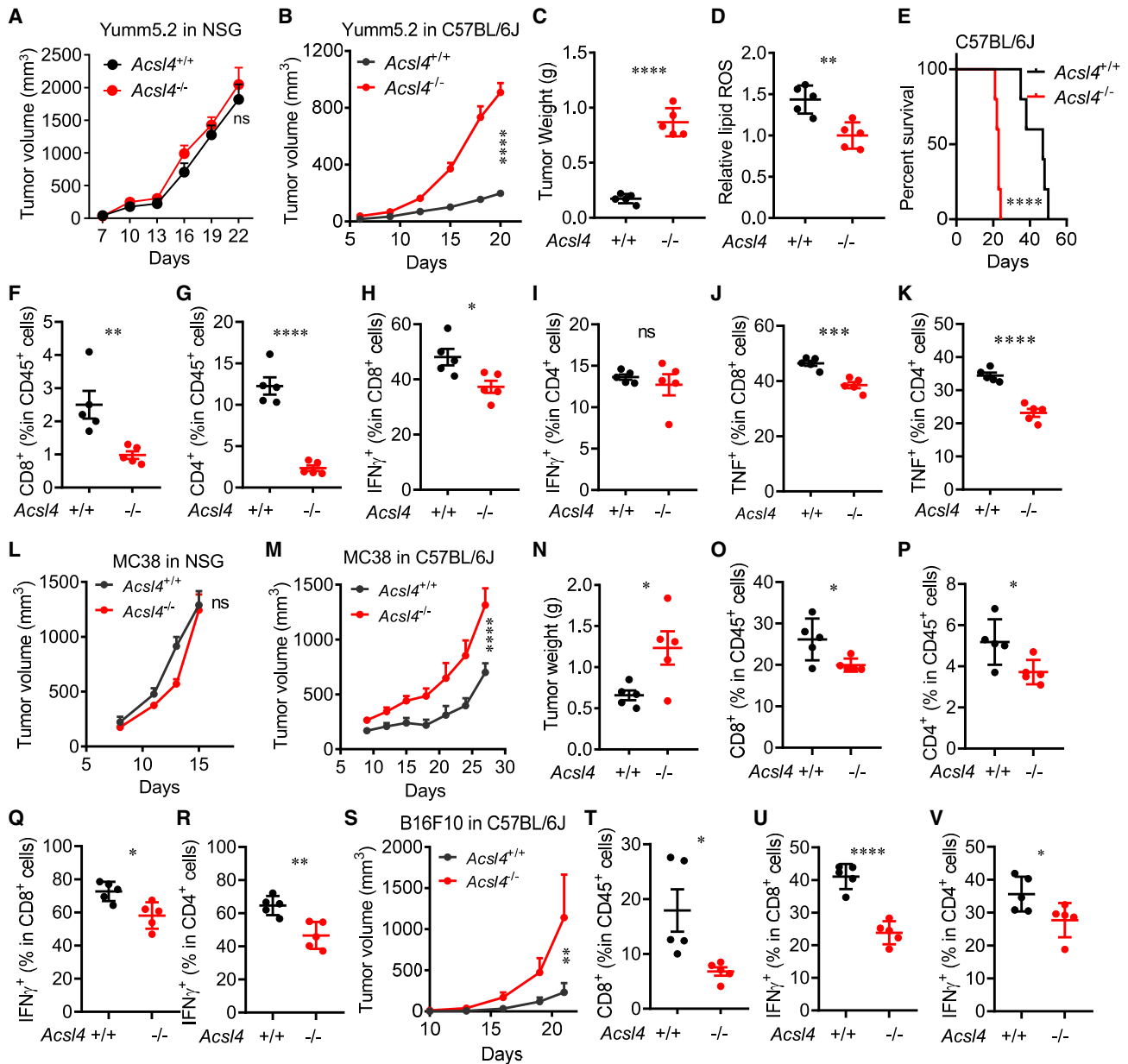
Figure 5. Tumor ACSL4 affects anti-tumor immunity

(A and B) Growth of *Acsl4*$^{+/+}$ or *Acsl4*$^{-/-}$ Yumm5.2 tumors in NSG mice (A) or C57BL/6 mice (B) (n = 5).

(C) Tumor weights of *Acsl4*$^{+/+}$ or *Acsl4*$^{-/-}$ Yumm5.2 tumors in C57BL/6 mice (n = 5).

(D) Relative lipid ROS in *Acsl4*$^{+/+}$ or *Acsl4*$^{-/-}$ Yumm5.2 tumors in C57BL/6 mice (n = 5).

(E) Overall survival of C57BL/6 mice bearing *Acsl4*$^{+/+}$ or *Acsl4*$^{-/-}$ Yumm5.2 tumors (n = 5).

(F and G) Percentages of CD8$^+$ (F) and CD4$^+$ (G) T cells in CD45$^+$ cells of Yumm5.2 tumors (n = 5).

(H–K) Percentages of IFNγ$^+$ (H and I) and TNFα$^+$ (J and K) in CD8$^+$ and CD4$^+$ T cells of Yumm5.2 tumors (n = 5).

(L and M) Growth of *Acsl4*$^{+/+}$ or *Acsl4*$^{-/-}$ MC38 tumors in NSG mice (L) or C57BL/6 (M) mice (n = 5–7).

(N) Tumor weights of *Acsl4*$^{+/+}$ or *Acsl4*$^{-/-}$ MC38 tumors in C57BL/6 mice (n = 5).

(O and P) Percentages of CD8$^+$ (O) and CD4$^+$ (P) T cells in CD45$^+$ cells of MC38 tumors (n = 5).

(Q and R) Percentages of IFNγ$^+$ CD8$^+$ (Q) and IFNγ$^+$ CD4$^+$ (R) T cells of MC38 tumors (n = 5).

(S) Growth of *Acsl4*$^{+/+}$ or *Acsl4*$^{-/-}$ B16F10 tumors in C57BL/6 mice (n = 5).

(T) Percentages of CD8$^+$ T cells in CD45$^+$ cells of B16F10 tumors (n = 5).

(U and V) Percentages of IFNγ$^+$ CD8$^+$ (U) and IFNγ$^+$ CD4$^+$ (V) T cells of B16F10 tumors (n = 5). Data are shown as mean ± SEM (A–C and G–I), two-way ANOVA(A, B, L, M, and S), two-tailed t-test (C, D, F–K, N–R, and T–V) or log rank test (E), *p < 0.05, **p < 0.01, ***p < 0.001, ****p < 0.0001; ns, not significant.

See also Figure S4.
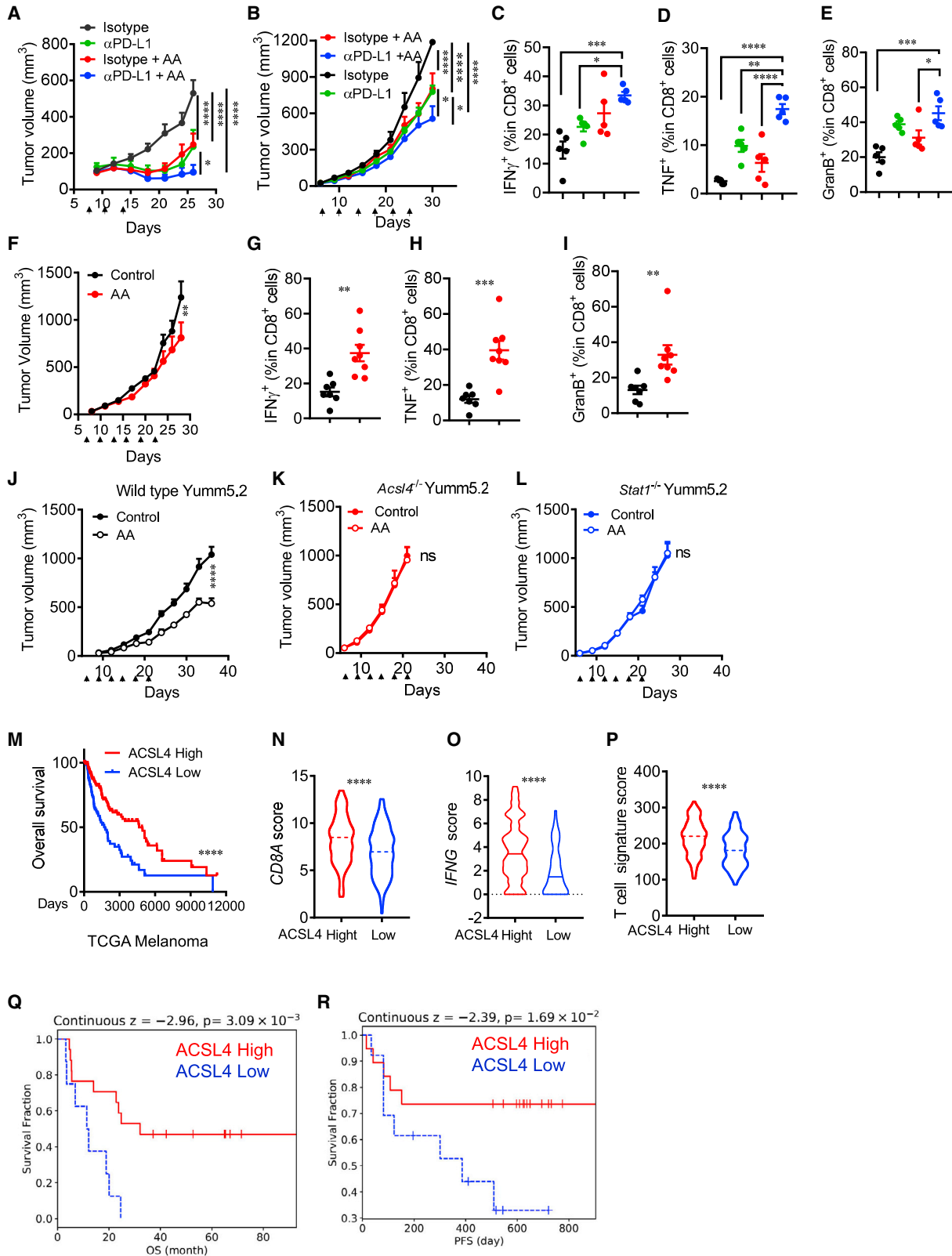
(legend on next page)

tumor microenvironment (Figures 6G–6I). Moreover, treatment with arachidonic acid failed to affect tumor growth in NSG mice bearing MC38 (Figure S5B), Yumm5.2 (Figure S5C), and LLC (Figure S5D) tumors. In addition to tumor cells, low-dose arachidonic acid may directly alter T cell survival, function, and lipid profile. To test this, we stimulated T cells *in vitro* in the presence of arachidonic acid. We found that arachidonic acid treatment had no effect on T cell death and function, as shown by 7-AAD, intracellular IL-2, and granzyme B staining, respectively (Figure S5E and S5F). Then, we treated Yumm5.2 tumor-bearing mice with low-dose arachidonic acid and isolated T cells for functional test and lipidomic assay. In line with the *in vitro* data (Figures S5E and S5F), arachidonic acid treatment had no obvious effects on T cell death and expression of IL-2 and granzyme B (Figures S5G and S5H). Lipidomic assay demonstrated similar phospholipid patterns in T cells isolated from mice treated with or without arachidonic acid (Figures S5I–S5P). Thus, low-dose arachidonic acid targets tumors, promotes tumor immunity, and sensitizes therapeutic efficacy to checkpoint blockade.

We next assessed whether the anti-tumor effect mediated by arachidonic acid administration depended on tumor ACSL4 and IFNγ signal pathway. To this end, we treated mice bearing wild-type, $Acsl4^{-/-}$, and $Stat1^{-/-}$ Yumm5.2 tumors with arachidonic acid. As expected, administration of arachidonic acid slowed down wild-type tumor growth but had no effect on $Acsl4^{-/-}$ and $Stat1^{-/-}$ Yumm5.2 tumors, as shown by tumor volume and tumor mass images (Figures 6J–6L and S5Q–S5S). These results suggest that the therapeutic effect of arachidonic acid is ACSL4 and IFNγ signaling dependent.

Finally, we assessed the potential relevance of ACSL4 in human tumor immunity. We first compared transcript levels of ACSL4 between normal tissues and tumor tissues in patients with cancer. Using TIMER2.0 analysis, we found that ACSL4 expression levels were lower in multiple types of tumor tissues than in normal tissues (Li et al., 2020) (Figure S6A). We next examined the relationship between *ACSL4* expression, cancer patient outcome, and immune signatures. On the basis of gene expression profiles of cancer patients from The Cancer Genome Atlas (TCGA) database and Kaplan-Meier survival analysis, we found that high *ACSL4* expression was associated with improved overall survival in patients with melanoma (Figure 6M) and bladder cancer (Figure S6B). ACSL4 expression positively

correlated with CD8A (Figures 6N and S6C), IFNγ (Figures 6O and S6D), and T cell signature (Ayers et al., 2017) (Figures 6P and S6E). Then, we employed Tumor Immune Dysfunction and Exclusion (TIDE) algorithm (Jiang et al., 2018) to assess the relationship between tumor ACSL4 expression and clinical response to immunotherapy (Gide et al., 2019; Lauss et al., 2017). We observed that high levels of ACSL4 expression were associated with increased overall survival or progression free survival in patients having received immunotherapy (Figures 6Q and 6R). The data suggest a potential involvement of ACSL4 in spontaneous and ICB-induced anti-tumor immunity in patients with cancer.

DISCUSSION

Ferroptosis inducers are synthetic molecules that decrease tumor growth (Dixon and Stockwell, 2019). It is not clear whether activation of endogenous ferroptosis mechanisms restricts tumor progression and alters checkpoint therapy sensitivity. Here, we find that ACSL4 is the lynchpin that activates endogenous ferroptotic mechanisms through metabolic lipid reprogramming. Moreover, IFNγ in combination with arachidonic acid directly triggers ferroptosis in both human and mouse tumor cells and serves as a mode of action for CTL-tumor killing.

Arachidonic acid (20:4) is an omega-6, polyunsaturated fatty acid. We detect moderate levels of arachidonic acid in the tumor microenvironment. Arachidonic acid can enhance RSL3-induced ferroptosis in mouse embryonic fibroblasts *in vitro*. However, arachidonic acid alone fails to directly initiate ferroptosis (Kagan et al., 2017). Similarly to arachidonic acid, IFNγ targets the X_c^- system and promotes synthetic-molecule-induced ferroptosis in human and mouse tumor cell lines (Wang et al., 2019). However, IFNγ alone is unable to directly trigger ferroptosis (Wang et al., 2019). Unlike each alone, the combination of arachidonic acid and IFNγ directly triggers tumor cell ferroptosis. This natural tumor ferroptotic mechanism is conceptually similar to the fundamental findings that the combination of different cytokines (such as TGFβ plus IL-6) induces Th17 cells or Th22 cells (Cua et al., 2003; Mangan et al., 2006; Zheng et al., 2007), and the combination of TNFα and IFNγ induces PANoptosis as characterized by inflammatory cell death (Karki et al., 2021). Thus, our results will stimulate a bridge of interest in exploring whether this mechanism is operative not only in tumor immunity but also

Figure 6. Targeting tumor ferroptosis sensitizes checkpoint therapy
(A) Effect of AA and anti-PD-L1 on MC38 tumor growth. Mice bearing subcutaneous MC38 tumors were treated with isotype antibody, anti-PD-L1 antibody, AA, or anti-PD-L1 antibody plus AA (arrowhead). Tumor volume is shown (n = 5).
(B–E) Effects of AA and anti-PD-L on Yumm5.2 tumor growth and immune responses. Yumm5.2 tumor-bearing mice were treated with isotype antibody, anti-PD-L1 antibody, AA, or anti-PD-L1 plus AA (arrowhead). Tumor volume is shown (B). Percentages of tumor infiltrating IFNγ$^+$ (C), TNFα$^+$ (D), and granzyme B$^+$ (E) CD8$^+$ T cells were analyzed by FACS (n = 5).
(F–I) Effects of AA administration on LLC tumor growth and immune responses. LLC tumor-bearing mice were treated with PBS, (Control) and AA (arrowhead). Tumor volume is shown (F). Percentages of tumor-infiltrating IFNγ$^+$ (G), TNFα$^+$ (H), and granzyme B$^+$ (I) CD8$^+$ T cells were analyzed by FACS (n = 7–8).
(J–L) Effect of AA administration on tumor growth *in vivo*. Wild-type (J), $Acsl4^{-/-}$(K), and $Stat1^{-/-}$ (L) Yumm5.2 tumor-bearing mice were treated with PBS and AA (arrowhead). Tumor volume is shown (n = 8–9).
(M) Kaplan-Meier survival curves for melanoma patients with low (bottom 25%) or high (top 25%) melanoma ACSL4 transcripts in TCGA dataset.
(N–P) Correlation between ACSL4 transcripts and immune genes, including CD8A (N), IFNG (O), and T cell signature (P) in TCGA dataset in patients with melanoma expressing high (n = 120) or low (n = 120) levels of ACSL4. Dotted lines, median.
(Q and R) Kaplan-Meier survival curves for melanoma patients having received adoptive T cell therapy (ACT) with high (n = 17) and low (n = 8) levels of tumor ACSL4 transcripts (Lauss et al., 2017)(Q) or having received the combination of anti-PD-1 and anti-CTLA-4 with high (n = 19) and low (n = 13) levels of tumor ACSL4 transcripts (Gide et al., 2019)(R). Data are shown as mean ± SEM, two-way ANOVA(A, B, F, and J-L), one-way ANOVA(C–E), two-tailed t test (G–I and N–P) or log rank test (M, Q, and R), *p < 0.05, **p < 0.01, ***p < 0.001, ****p < 0.0001; ns, not significant.
See also Figures S5 and S6.

in autoimmunity and infection immunity. In addition, as IFNγ is often produced by activated effector T cells, anemic T cell infiltration and loss of IFNγ gene signaling can result in bypassing the aforementioned natural immune-related tumor ferroptotic mechanism, leading to tumor progression. Hence, our data suggest that natural tumor ferroptosis deficiency may be a previously unrecognized feature of cold tumors.

Ferroptosis occurs when lipid hydroperoxide detoxification and accumulation is unbalanced (Dixon and Stockwell, 2019). Environmental stress may tip this balance in favor of lipid ROS accumulation, resulting in ferroptosis initiation (Wang et al., 2019). We posit that T cells function as an immune stress signal to tumor cells, thereby resulting in ferroptotic tumor cell death and subsequent tumor antigen release and T cell activation in the tumor microenvironment. In support of this notion, we demonstrate that cross talk between the IFNγ and ACSL4 signaling pathways contributes to CTL-mediated tumor cell death via inducing ferroptosis. It is well known that CTLs kill targets via the perforin-granzyme-caspase-mediated apoptosis (Voskoboinik et al., 2015). Our results show that ACSL4-dependent ferroptosis is a previously unappreciated mode of action of CTLs. Thus, CTL-induced tumor apoptosis is no longer a soloist in this process. Given that cell apoptosis is generally considered an immune tolerogenic cell death ("type 2 cell death"), we suggest that tumor ferroptosis induced by the combination of IFNγ and arachidonic acid is the long-awaited form of immunogenic cell death ("type 1 cell death"). Our finding not only sheds light on CTL-killing mechanisms but also raises the possibility of a potential interplay between two types of cell death, namely, ferroptosis and apoptosis.

Arachidonic acid is a conditionally essential polyunsaturated long-chain fatty acid (PUFA) (Harizi et al., 2008; Tallima and El Ridi, 2018). ACSL4 preferentially uses PUFAs, including arachidonic acid, as substrates (Dixon et al., 2015; Doll et al., 2017). ACSL4 activates arachidonic acid by thioesterification with coenzyme A (CoA), generating arachidonyl-CoA, the first-step reaction of arachidonic acid metabolism (Kagan et al., 2017). Lysophosphatidylcholine acyltransferase 3 (LPCAT3) and lipoxygenases (LOX) are involved in the incorporation of arachidonyl-CoAs into phospholipids on membranes and oxidation of these phospholipids, respectively (Conrad and Pratt, 2019; Ingold et al., 2018; Wenzel et al., 2017). Hence, ACSL4 plays an essential role in PUFA metabolism. Unexpectedly, we have found cross talk between the ACSL4-mediated PUFA metabolic pathway and the IFNγ signaling pathway in tumor cells. IFNγ targets the promotor region of ACSL4 and transcriptionally stimulates ACSL4 expression in tumor cells. Furthermore, IFNγ alters the tumor cell lipidomic pattern in the presence of arachidonic acid via ACSL4. IFNγ increases the total arachidonic acid-associated phospholipid species, particularly C16 and C18 acyl chain-containing phospholipids. This suggests the involvement of C16 and C18 fatty acid-associated phospholipids in tumor cell ferroptosis. In line with this possibility, we demonstrate that the common C16 and C18 fatty acids in peripheral blood, such as POA and OA, can enhance tumor ferroptosis initiated by the combination of IFNγ and arachidonic acid via ACSL4, and OA enhances key arachidonic acid-d5-incorporated lipid species of PE and PC in tumor cells. The data indicate that T cells can selectively reprogram lipid metabolism in tumor cells via the IFNγ signaling pathway. Future

studies are essential to explore thoroughly the unknown roles and modes of action of many individual fatty acids and their combinations in spontaneous and ICB-associated tumor cell ferroptosis. Along this line, metabolic reprogramming occurs in tumorigenesis (Boroughs and DeBerardinis, 2015) and cancer immunotherapy (Li et al., 2019). Lipid metabolism, including fatty acid and cholesterol metabolism, can affect CD8$^+$ T cell activity and is involved in the regulation of T cell immunity induced by cancer immunotherapy (Ma et al., 2019; Pearce et al., 2009; Yang et al., 2016a; Zhang et al., 2017). Given moderate levels of arachidonic acid in the tumor microenvironment and its role in tumor ferroptosis, we reason that supplementation of arachidonic acid may stimulate tumor ferroptosis *in vivo* and synergize checkpoint therapy. Indeed, low-dose arachidonic acid administration inhibits growth of multiple murine tumors *in vivo* in immunocompetent models, including mouse LLC tumor, an ICB-resistant tumor. Additionally, administration of low-dose arachidonic acid has the ability to enhance the therapeutic efficacy of PD-L1 blockade and elevate the anti-tumor T cell response via the IFNγ signaling pathway. Thus, ICB-triggered IFNγ signaling can cooperate with arachidonic acid to induce and enhance tumor ferroptosis, resulting in effective tumor regression. Thus, targeting arachidonic acid metabolism may be a previously unappreciated approach to synergize with cancer immune checkpoint blockade.

STAR★METHODS

Detailed methods are provided in the online version of this paper and include the following:

- KEY RESOURCES TABLE
- RESOURCE AVAILABILITY
  - Lead contact
  - Materials availability
  - Data and code availability
- EXPERIMENTAL MODEL AND SUBJECT DETAILS
  - Cell lines
  - Animal models
- METHOD DETAILS
  - Generation of ACSL4$^{-/-}$ and STAT1$^{-/-}$ tumor cells
  - OT-I cell isolation and co-culture with OVA$^+$ tumor cells
  - BODIPY-C11 staining
  - Targeted phospholipid analysis
  - Quantification of arachidonic acid
  - Quantification of prostaglandin E2 (PGE2)
  - Cell death measurement and immune profiling by FACS
  - Cell proliferation and viability assay
  - Quantitative PCR analysis
  - Immunoblotting
  - Chromatin immunoprecipitation (ChIP)
  - *In vitro* T cell activation
  - Mouse T cell isolation
- QUANTIFICATION AND STATISTICAL ANALYSIS

SUPPLEMENTAL INFORMATION

Supplemental information can be found online at https://doi.org/10.1016/j.ccell.2022.02.003.

Cancer Cell
Article

AUTHOR CONTRIBUTIONS

P.L., Weimin W., and W.Z. conceived the idea, designed the experiments, and composed the paper. P.L. WeiminW., and Weichao W. conducted experiments; I.K. assisted in FACS analysis; X.L. assisted in bioinformatics analysis; S.W. and S.G. assisted in animal experiments; Y.B. assisted in isolation of T cells; A.S. assisted in qPCR; J.J., P.D.K., and M.G. assisted in LC-MS/MS analysis. P.L., Weimin W., I.K., Y.S., and W.Z. contributed to the interpretation of the results. W.Z. supervised the project.

DECLARATION OF INTERESTS

The authors declare no competing interests.

REFERENCES

Ayers, M., Lunceford, J., Nebozhyn, M., Murphy, E., Loboda, A., Kaufman, D.R., Albright, A., Cheng, J.D., Kang, S.P., Shankaran, V., et al. (2017). IFN-gamma-related mRNA profile predicts clinical response to PD-1 blockade. J. Clin. Invest. *127*, 2930–2940.

Bersuker, K., Hendricks, J.M., Li, Z., Magtanong, L., Ford, B., Tang, P.H., Roberts, M.A., Tong, B., Maimone, T.J., Zoncu, R., et al. (2019). The CoQ oxidoreductase FSP1 acts parallel to GPX4 to inhibit ferroptosis. Nature *575*, 688–692.

Boroughs, L.K., and DeBerardinis, R.J. (2015). Metabolic pathways promoting cancer cell survival and growth. Nat. Cell Biol. *17*, 351–359.

Bottcher, J.P., Bonavita, E., Chakravarty, P., Blees, H., Cabeza-Cabrerizo, M., Sammicheli, S., Rogers, N.C., Sahai, E., Zelenay, S., and Reis e Sousa, C. (2018). NK cells stimulate recruitment of cDC1 into the tumor microenvironment promoting cancer immune control. Cell *172*, 1022–1037.e4.

Conrad, M., and Pratt, D.A. (2019). The chemical basis of ferroptosis. Nat. Chem. Biol. *15*, 1137–1147.

Consortium, E.P. (2012). An integrated encyclopedia of DNA elements in the human genome. Nature *489*, 57–74.

Cua, D.J., Sherlock, J., Chen, Y., Murphy, C.A., Joyce, B., Seymour, B., Lucian, L., To, W., Kwan, S., Churakova, T., et al. (2003). Interleukin-23 rather than interleukin-12 is the critical cytokine for autoimmune inflammation of the brain. Nature *421*, 744–748.

Dixon, S.J., and Stockwell, B.R. (2019). The hallmarks of ferroptosis. Annu. Rev. Canc Biol. *3*, 35–54.

Dixon, S.J., Winter, G.E., Musavi, L.S., Lee, E.D., Snijder, B., Rebsamen, M., Superti-Furga, G., and Stockwell, B.R. (2015). Human haploid cell genetics reveals roles for lipid metabolism genes in nonapoptotic cell death. ACS Chem. Biol. *10*, 1604–1609.

Doll, S., Freitas, F.P., Shah, R., Aldrovandi, M., da Silva, M.C., Ingold, I., Grocin, A.G., da Silva, T.N.X., Panzilius, E., Scheel, C.H., et al. (2019). FSP1 is a glutathione-independent ferroptosis suppressor. Nature *575*, 693.

Doll, S., Proneth, B., Tyurina, Y.Y., Panzilius, E., Kobayashi, S., Ingold, I., Irmler, M., Beckers, J., Aichler, M., Walch, A., et al. (2017). ACSL4 dictates ferroptosis sensitivity by shaping cellular lipid composition. Nat. Chem. Biol. *13*, 91–98.

Farrar, M.A., and Schreiber, R.D. (1993). The molecular cell biology of interferon-gamma and its receptor. Annu. Rev. Immunol. *11*, 571–611.

Gide, T.N., Quek, C., Menzies, A.M., Tasker, A.T., Shang, P., Holst, J., Madore, J., Lim, S.Y., Velickovic, R., Wongchenko, M., et al. (2019). Distinct immune cell populations define response to anti-PD-1 monotherapy and anti-PD-1/anti-CTLA-4 combined therapy. Cancer Cell *35*, 238–255.e6.

Golej, D.L., Askari, B., Kramer, F., Barnhart, S., Vivekanandan-Giri, A., Pennathur, S., and Bornfeldt, K.E. (2011). Long-chain acyl-CoA synthetase 4 modulates prostaglandin E(2) release from human arterial smooth muscle cells. J. Lipid Res. *52*, 782–793.

Harizi, H., Corcuff, J.B., and Gualde, N. (2008). Arachidonic-acid-derived eicosanoids: roles in biology and immunopathology. Trends Mol. Med. *14*, 461–469.

Hassannia, B., Vandenabeele, P., and Vanden Berghe, T. (2019). Targeting ferroptosis to iron out cancer. Cancer Cell *35*, 830–849.

Ingold, I., Berndt, C., Schmitt, S., Doll, S., Poschmann, G., Buday, K., Roveri, A., Peng, X., Porto Freitas, F., Seibt, T., et al. (2018). Selenium utilization by GPX4 is required to prevent hydroperoxide-induced ferroptosis. Cell *172*, 409–422.e1.

Jiang, P., Gu, S., Pan, D., Fu, J., Sahu, A., Hu, X., Li, Z., Traugh, N., Bu, X., Li, B., et al. (2018). Signatures of T cell dysfunction and exclusion predict cancer immunotherapy response. Nat. Med. *24*, 1550–1558.

Kagan, V.E., Mao, G., Qu, F., Angeli, J.P., Doll, S., Croix, C.S., Dar, H.H., Liu, B., Tyurin, V.A., Ritov, V.B., et al. (2017). Oxidized arachidonic and adrenic PEs navigate cells to ferroptosis. Nat. Chem. Biol. *13*, 81–90.

Karki, R., Sharma, B.R., Tuladhar, S., Williams, E.P., Zalduondo, L., Samir, P., Zheng, M., Sundaram, B., Banoth, B., Malireddi, R.K.S., et al. (2021). Synergism of TNF-alpha and IFN-gamma triggers inflammatory cell death, tissue damage, and mortality in SARS-CoV-2 infection and cytokine shock syndromes. Cell *184*, 149–168.e7.

Kim, J.H., Lewin, T.M., and Coleman, R.A. (2001). Expression and characterization of recombinant rat Acyl-CoA synthetases 1, 4, and 5. Selective inhibition by triacsin C and thiazolidinediones. J. Biol. Chem. *276*, 24667–24673.

Kraft, V.A.N., Bezjian, C.T., Pfeiffer, S., Ringelstetter, L., Muller, C., Zandkarimi, F., Merl-Pham, J., Bao, X.W., Anastasov, N., Kossl, J., et al. (2020). GTP cyclohydrolase 1/tetrahydrobiopterin counteract ferroptosis through lipid remodeling. ACS Cent. Sci. *6*, 41–53.

Kuwata, H., Nakatani, E., Shimbara-Matsubayashi, S., Ishikawa, F., Shibanuma, M., Sasaki, Y., Yoda, E., Nakatani, Y., and Hara, S. (2019). Long-chain acyl-CoA synthetase 4 participates in the formation of highly unsaturated fatty acid-containing phospholipids in murine macrophages. Biochim. Biophys. Acta Mol. Cell Biol. Lipids *1864*, 1606–1618.

Lang, X., Green, M.D., Wang, W., Yu, J., Choi, J.E., Jiang, L., Liao, P., Zhou, J., Zhang, Q., Dow, A., et al. (2019). Radiotherapy and immunotherapy promote tumoral lipid oxidation and ferroptosis via synergistic repression of SLC7A11. Cancer Discov. *9*, 1673–1685.

Lauss, M., Donia, M., Harbst, K., Andersen, R., Mitra, S., Rosengren, F., Salim, M., Vallon-Christersson, J., Torngren, T., Kvist, A., et al. (2017). Mutational and putative neoantigen load predict clinical benefit of adoptive T cell therapy in melanoma. Nat. Commun. *8*, 1738.

Li, T., Fu, J., Zeng, Z., Cohen, D., Li, J., Chen, Q., Li, B., and Liu, X.S. (2020). TIMER2.0 for analysis of tumor-infiltrating immune cells. Nucleic Acids Res. *48*, W509–W514.

Li, X., Wenes, M., Romero, P., Huang, S.C., Fendt, S.M., and Ho, P.C. (2019). Navigating metabolic pathways to enhance antitumour immunity and immunotherapy. Nat. Rev. Clin. Oncol. *16*, 425–441.

Li, Y., Fang, M., Zhang, J., Wang, J., Song, Y., Shi, J., Li, W., Wu, G., Ren, J., Wang, Z., et al. (2016). Hydrogel dual delivered celecoxib and anti-PD-1 synergistically improve antitumor immunity. Oncoimmunology *5*, e1074374.

Lin, H., Wei, S., Hurt, E.M., Green, M.D., Zhao, L., Vatan, L., Szeliga, W., Herbst, R., Harms, P.W., Fecher, L.A., et al. (2018). Host expression of PD-L1 determines efficacy of PD-L1 pathway blockade-mediated tumor regression. J. Clin. Invest. *128*, 805–815.

Ma, X.Z., Bi, E.G., Lu, Y., Su, P., Huang, C.J., Liu, L.T., Wang, Q., Yang, M.J., Kalady, M.F., Qian, J.F., et al. (2019). Cholesterol induces CD8(+) T cell exhaustion in the tumor microenvironment. Cell Metab. *30*, 143.

Magtanong, L., Ko, P.J., To, M., Cao, J.Y., Forcina, G.C., Tarangelo, A., Ward, C.C., Cho, K., Patti, G.J., Nomura, D.K., et al. (2019). Exogenous

monounsaturated fatty acids promote a ferroptosis-resistant cell state. Cell Chem. Biol. *26*, 420–432 e429.

Mangan, P.R., Harrington, L.E., O'Quinn, D.B., Helms, W.S., Bullard, D.C., Elson, C.O., Hatton, R.D., Wahl, S.M., Schoeb, T.R., and Weaver, C.T. (2006). Transforming growth factor-beta induces development of the T(H)17 lineage. Nature *441*, 231–234.

Pearce, E.L., Walsh, M.C., Cejas, P.J., Harms, G.M., Shen, H., Wang, L.S., Jones, R.G., and Choi, Y. (2009). Enhancing CD8 T-cell memory by modulating fatty acid metabolism. Nature *460*, 103–107.

Peng, D., Kryczek, I., Nagarsheth, N., Zhao, L., Wei, S., Wang, W., Sun, Y., Zhao, E., Vatan, L., Szeliga, W., et al. (2015). Epigenetic silencing of TH1-type chemokines shapes tumour immunity and immunotherapy. Nature *527*, 249–253.

Psychogios, N., Hau, D.D., Peng, J., Guo, A.C., Mandal, R., Bouatra, S., Sinelnikov, I., Krishnamurthy, R., Eisner, R., Gautam, B., et al. (2011). The human serum metabolome. PLoS One *6*, e16957.

Reeves, A.R., Sansbury, B.E., Pan, M., Han, X., Spite, M., and Greenberg, A.S. (2021). Myeloid-specific deficiency of long-chain acyl CoA synthetase 4 reduces inflammation by remodeling phospholipids and reducing production of arachidonic acid-derived proinflammatory lipid mediators. J. Immunol. *207*, 2744–2753.

Sommerfeld, M. (1983). Trans unsaturated fatty acids in natural products and processed foods. Prog. Lipid Res. *22*, 221–233.

Tallima, H., and El Ridi, R. (2018). Arachidonic acid: physiological roles and potential health benefits - a review. J. Adv. Res. *11*, 33–41.

Voskoboinik, I., Whisstock, J.C., and Trapani, J.A. (2015). Perforin and granzymes: function, dysfunction and human pathology. Nat. Rev. Immunol. *15*, 388–400.

Wang, W., Green, M., Choi, J.E., Gijon, M., Kennedy, P.D., Johnson, J.K., Liao, P., Lang, X., Kryczek, I., Sell, A., et al. (2019). CD8(+) T cells regulate tumour ferroptosis during cancer immunotherapy. Nature *569*, 270–274.

Watson, M.J., Vignali, P.D.A., Mullett, S.J., Overacre-Delgoffe, A.E., Peralta, R.M., Grebinoski, S., Menk, A.V., Rittenhouse, N.L., DePeaux, K.,

Whetstone, R.D., et al. (2021). Metabolic support of tumour-infiltrating regulatory T cells by lactic acid. Nature *591*, 645.

Wenzel, S.E., Tyurina, Y.Y., Zhao, J., St Croix, C.M., Dar, H.H., Mao, G., Tyurin, V.A., Anthonymuthu, T.S., Kapralov, A.A., Amoscato, A.A., et al. (2017). PEBP1 wardens ferroptosis by enabling lipoxygenase generation of lipid death signals. Cell *171*, 628–641 e626.

Yang, W., Bai, Y., Xiong, Y., Zhang, J., Chen, S., Zheng, X., Meng, X., Li, L., Wang, J., Xu, C., et al. (2016a). Potentiating the antitumour response of CD8(+) T cells by modulating cholesterol metabolism. Nature *531*, 651–655.

Yang, W.S., Kim, K.J., Gaschler, M.M., Patel, M., Shchepinov, M.S., and Stockwell, B.R. (2016b). Peroxidation of polyunsaturated fatty acids by lipoxygenases drives ferroptosis. Proc. Natl. Acad. Sci. U S A. *113*, E4966–E4975.

Zabielski, P., Blachnio-Zabielska, A., Lanza, I.R., Gopala, S., Manjunatha, S., Jakaitis, D.R., Persson, X.M., Gransee, J., Klaus, K.A., Schimke, J.M., et al. (2014). Impact of insulin deprivation and treatment on sphingolipid distribution in different muscle subcellular compartments of streptozotocin-diabetic C57Bl/6 mice. Am. J. Physiol. Endocrinol. Metab. *306*, E529–E542.

Zelenay, S., van der Veen, A.G., Bottcher, J.P., Snelgrove, K.J., Rogers, N., Acton, S.E., Chakravarty, P., Girotti, M.R., Marais, R., Quezada, S.A., et al. (2015). Cyclooxygenase-dependent tumor growth through evasion of immunity. Cell *162*, 1257–1270.

Zhang, Y., Kurupati, R., Liu, L., Zhou, X.Y., Zhang, G., Hudaihed, A., Filisio, F., Giles-Davis, W., Xu, X., Karakousis, G.C., et al. (2017). Enhancing CD8(+) T cell fatty acid catabolism within a metabolically challenging tumor microenvironment increases the efficacy of melanoma immunotherapy. Cancer Cell *32*, 377–391.e9.

Zheng, Y., Danilenko, D.M., Valdez, P., Kasman, I., Eastham-Anderson, J., Wu, J.F., and Ouyang, W.J. (2007). Interleukin-22, a T(H)17 cytokine, mediates IL-23-induced dermal inflammation and acanthosis. Nature *445*, 648–651.

Zou, Y.L., Li, H.X., Graham, E.T., Deik, A.A., Eaton, J.K., Wang, W.Y., Sandoval-Gomez, G., Clish, C.B., Doench, J.G., and Schreiber, S.L. (2020). Cytochrome P450 oxidoreductase contributes to phospholipid peroxidation in ferroptosis. Nat. Chem. Biol. *16*, 302.

STAR★METHODS

KEY RESOURCES TABLE

REAGENT or RESOURCE	SOURCE	IDENTIFIER
Antibodies		
Recombinant Anti-FACL4 antibody [EPR8640]	Abcam	Cat# ab155282, RRID:AB_2714020
Anti-ACSL4 Antibody	Santa Cruz	Cat# sc-271800, RRID:AB_10715092
Stat1 (42H3) Rabbit mAb	Cell Signaling Technology	Cat# 9175, RRID:AB_2197984
IRF-1 (D5E4) XP® Rabbit mAb	Cell Signaling Technology	Cat# 8478, RRID:AB_10949108
β-Actin (13E5) Rabbit mAb	Cell Signaling Technology	Cat# 5125, RRID:AB_1903890
xCT/SLC7A11 Antibody	Cell Signaling Technology	Cat# 98051, RRID:AB_2800296
Normal Rabbit IgG antibody	Cell Signaling Technology	Cat# 2729, RRID:AB_1031062
V500 Rat Anti-Mouse CD45 (30-F11)	BD Bioscience	Cat# 561487; RRID: AB_10697046
FITC Rat Anti-Mouse CD90.2 (53-2.1)	BD Bioscience	Cat# 553003; RRID: AB_394542
Alexa Fluor® 700 Rat Anti-Mouse CD8a (53-6.7)	BD Bioscience	Cat# 557959; RRID: AB_396959
BV786 Rat Anti-Mouse IFNγ (XMG1.2)	BD Bioscience	Cat# 563773; RRID: AB_2738419
PE-Cy™7 Rat Anti-Mouse TNF (MP6-XT22)	BD Bioscience	Cat# 557644; RRID: AB_396761
PE Mouse Anti-Human Granzyme B (GB11)	BD Bioscience	Cat# 561142; RRID: AB_10561690
Armenian hamster Anti-Mouse CD3e (145-2C11)	Thermo Fisher	Cat# 14-0031-82; RRID: AB_467048
Syrian hamster Anti-Mouse CD28 (37.51)	Thermo Fisher	Cat# 14-0281-82; RRID: AB_466413
PE Mouse anti-OVA257-264 (SIINFEKL) peptide bound to H-2Kb (eBio25-D1.16)	Thermo Fisher	Cat# 12-5743-82; RRID: AB_925771
InVivoMAb rat IgG2a isotype control (2A3)	Bio X Cell	Cat# BE0089; RRID: AB_1107769
InVivoPlus Anti-mouse PD-L1 (10F.9G2)	Bio X Cell	Cat# BE0101; RRID: AB_10949073
IFN gamma Monoclonal Antibody (XMG1.2)	Thermo Fisher	Cat# 16-7311-85
TNF alpha Monoclonal Antibody (MP6-XT22)	Thermo Fisher	Cat# 14-7321-81
Rat IgG1 kappa Isotype Control (eBRG1)	Thermo Fisher	Cat# 16-4301-81
Chemicals, peptides, and recombinant proteins		
Formic acid	Sigma-Aldrich	Cat# 695076
Acetic acid	Sigma-Aldrich	Cat# A6283
Propionic acid	Sigma-Aldrich	Cat# P1386
Butyric acid	Sigma-Aldrich	Cat# B103500
Isobutyric acid	Sigma-Aldrich	Cat# I1754
Valeric acid	Sigma-Aldrich	Cat# 240370
Isovaleric acid	Sigma-Aldrich	Cat# 129542
Hexanoic acid	Sigma-Aldrich	Cat# 153745
Octanoic acid	Sigma-Aldrich	Cat# C2875
Decanoic acid	Sigma-Aldrich	Cat# C1875
Arachidonic acid	Cayman Chemical	Cat# 90010
Arachidonic Acid (peroxide free)	Cayman Chemical	Cat# 90010.1
Oleic acid	Cayman Chemical	Cat# 90260
Linoleic Acid	Cayman Chemical	Cat# 90150
γ-linolenic acid	Cayman Chemical	Cat# 90220
Palmitic acid	Cayman Chemical	Cat# 10006627
Elaidic acid	Cayman Chemical	Cat# 90250
Palmitoleic acid	Cayman Chemical	Cat# 10009871

(Continued on next page)

Continued

REAGENT or RESOURCE	SOURCE	IDENTIFIER
α-linolenic acid	Cayman Chemical	Cat# 90210
Stearic acid	Cayman Chemical	Cat# 10011298
Trans-vaccenic acid	Cayman Chemical	Cat# 15301
Lauric acid	Cayman Chemical	Cat# 10006626
Myristic acid	Cayman Chemical	Cat# 13351
Myristoleic acid	Cayman Chemical	Cat# 9002461
13(Z)-docosenoic acid	Cayman Chemical	Cat# 90175
Docosanoic acid	Cayman Chemical	Cat# 9000338
Lignoceric acid	Cayman Chemical	Cat# 13353
Hexacosanoic acid	Cayman Chemical	Cat# 13354
Octadecenoic acid	Cayman Chemical	Cat# 20026
Octacosanoic acid	Cayman Chemical	Cat# 31735
Nervonic acid	Cayman Chemical	Cat# 13940
(1S,3R)-RSL3 (RSL3)	Cayman Chemical	Cat# 19288
Erastin	Cayman Chemical	Cat# 17754
Ferrostatin-1	Cayman Chemical	Cat# 17729
Necrostatin-1	Cayman Chemical	Cat# 11658
Z-VAD(OH)-fmk	Cayman Chemical	Cat# 14467
Cisplatin	Cayman Chemical	Cat# 13119
Rosiglitazone	Cayman Chemical	Cat# 71740
2-Mercaptoethanol	Sigma-Aldrich	Cat# 63689
Ovalbumin Peptide (257-264) chicken	Sigma-Aldrich	Cat# S7951
Recombinant mouse IFNγ	R&D Systems	Cat# 485-MI
BODIPY™ 581/591 C11 (Lipid Peroxidation Sensor)	Thermo Fisher	Cat# D3861
BODIPY™ 665/676 (Lipid Peroxidation Sensor)	Thermo Fisher	Cat# B3932
7-AAD (7-Aminoactinomycin D)	Thermo Fisher	Cat# A1310
PI (Propidium Iodide)	Thermo Fisher	Cat# P1304MP
Deposited data		
Raw and analyzed lipidomic data	This paper	https://doi.org/10.17632/kvp23k439m.1
Gene expression profile of patient samples	(Lauss et al., 2017)	GEO dataSets: GSE100797
Gene expression profile of patient samples	(Gide et al., 2019)	ENA: PRJEB23709
Critical commercial assays		
Arachidonic Acid (AA) ELISA Kit	BioVision	Cat# E4602
Prostaglandin E2 (PGE2) Express ELISA Kit	Cayman Chemical	Cat# 500141
SimpleChIP® Enzymatic Chromatin IP Kit (Magnetic Beads)	Cell Signaling Technology	Cat# 9003
Experimental models: Cell lines		
Mouse cell line: YUMM5.2	ATCC	Cat# CRL-3367
Mouse cell line: B16-F10	ATCC	Cat# CRL-6475
Mouse cell line: LLC	ATCC	Cat# CRL-1642
Mouse cell line: MC38	(Lin et al., 2018)	N/A
Human cell line: A375	ATCC	Cat# CRL-1619
Experimental models: Organisms/strains		
Mouse: NOD.SCID γc deficient (NSG)	The Jackson Laboratory	Cat# JAX: 005557
Mouse: C57BL/6J	The Jackson Laboratory	Cat# JAX: 000664
Mouse: OT-I TCR transgenic mice	The Jackson Laboratory	Cat# JAX: 003831

REAGENT or RESOURCE	SOURCE	IDENTIFIER
Continued		
Oligonucleotides		
ChIP-qPCR primers		listed in Table S3
ACSL4 Double Nickase Plasmid (m)	Santa Cruz	Cat# sc-424503-NIC
STAT1 Double Nickase Plasmid (m)	Santa Cruz Biotechnology	Cat# sc-423174-NIC
Recombinant DNA		
Acsl4 (NM_207625) Mouse Tagged ORF Clone	Origene™ Technologies	Cat#MR210200
pLV[TetOn]-Puro-TRE3G>mAcsl4 [NM_207625.2]/3xFLAG	VectorBuilder	N/A
Software and algorithms		
Metabolomics Workbench	(Zabielski et al., 2014)	https://www.metabolomicsworkbench.org/
BD FACSDiva™ Software	BD Bioscience	https://www.bdbiosciences.com/en-us/products/software/instrument-software/bd-facsdiva-software#Overview
Graphpad Prism 8.0 software	GraphPad Software, Inc.	http://www.graphpad.com/scientific-software/prism/
ImageJ		https://imagej.nih.gov/ij/
Timer 2.0	(Li et al., 2020)	http://timer.cistrome.org/
TIDE	(Jiang et al., 2018)	http://tide.dfci.harvard.edu/

RESOURCE AVAILABILITY

Lead contact
Further information and requests for materials should be directed to the lead contact: Weiping Zou (wzou@med.umich.edu).

Materials availability
This study did not generate new unique reagents

Data and code availability
Lipidomic raw data and files have been deposited to Mendeley: https://doi.org/10.17632/kvp23k439m.1

Gene expression profiles of human cancer tissues were from GSE100797 (Lauss et al., 2017) and PRJEB23709 (Gide et al., 2019).

EXPERIMENTAL MODEL AND SUBJECT DETAILS

Cell lines
Human melanoma cell line A375 (CRL-1619), mouse melanoma cell lines, Yumm5.2 (CRL-3367), B16F10 (CRL-6475) and Lewis lung cancer cell (LLC) (CRL-1642) lines were purchased from the American Type Culture Collection (ATCC, Manassas, VA). Mouse colon cancer cell line MC38 was previously reported (Lin et al., 2018). Tumor cells were maintained in RPMI1640 (HyClone SH30255, GE Healthcare, Chicago, IL) containing 5% (v/v) fetal calf serum (Fcs) (HyClone, SH3007003HI) and 1% (v/v) pen/strep (GIBCO, 15140-122) for 30 generations or more than 3 months before performing experiments. All cell lines in our laboratory are routinely tested for mycoplasma contamination and cells used in this study were negative for mycoplasma. None of our cell lines are on the list of commonly misidentified cell lines (International Cell Line Authentication Committee). Tumor cells were treated with IFNγ (10 ng/ml) and arachidonic acid (AA) (20 μM) for 48-72 hours, unless otherwise specifically described.

To generate OVA-expressing mouse tumor cells, Yumm5.2 cells were transfected with the plasmid pCI-neo-mOVA (Addgene plasmid # 25099) and selected with 1 mg/mL G418 (Thermo Fisher) for 2 weeks.

Mouse CD8$^+$ T cells were isolated from spleen and lymph nodes using EasySep™ Mouse CD8$^+$ T Cell Isolation Kit (Stemcell Technologies, Cambridge, MA), and then stimulated with anti-CD3 (Clone 145-2C11, BD Biosciences, San Jose, CA) and anti-CD28 (Clone 37.51, BD Biosciences) for 3 days. T cell supernatant was collected by centrifugation at 3,000 ×g for 10 minutes and followed by filtration using a 0.2 μM filter.

Animal models
Six- to eight-week-old NOD.SCID γc-deficient (NSG) or C57BL/6 mice were obtained from The Jackson Laboratory. Mice were maintained under pathogen-free conditions. Tumor cells were cultured in the presence of 5% Fcs for 30 generations. Yumm5.2 tumor cells

(10^5), MC38 tumor cells (3.5×10^6), B16F10 tumor cells (5×10^4), and LLC tumor cells (10^5) were subcutaneously injected on the right flank of C57BL/6 mice. On day 6, 100 μg isotype control antibody or 100 μg anti-PD-L1 (Bio X Cell, NH) were peritoneally injected into tumor bearing mice. Tumor diameters were measured using calipers. Tumor volume was calculated as previously described (Peng et al., 2015). On day 6, arachidonic acid (peroxide free) $(C_{20}H_{32}O_2)$ (Cayman Chemical, 90010.1) (2 mg/kg) was administered intraperitoneally every three days. All animal studies were conducted under the approval of the University of Michigan Institutional Animal Care and Use Committee (PRO00010169).

METHOD DETAILS

Generation of ACSL4^{-/-} and STAT1^{-/-} tumor cells

ACSL4^{-/-} and STAT1^{-/-} cells were generated with CRISPR technology. Mouse ACSL4 and STAT1 loci were targeted by ACSL4 (Santa Cruz Biotechnology, sc 424503-NIC) and STAT1 (sc-423174-NIC) Double Nickase Plasmids (m) in Yumm5.2, MC38 and B16F10 cells using TurboFect[TM] (Thermo Fisher Scientific, R0532). 24 hours after transfection, cells were selected with 0.5-3 μg/ml puromycin (Santa Cruz Biotechnology, sc-108071C) for additional 96 hours. Single cell clones were selected and expanded in 96-well plate. Knockout clones were identified by immunoblotting. Multiple clones were pooled for the experiments.

OT-I cell isolation and co-culture with OVA^{+} tumor cells

C57BL/6-Tg (TcraTcrb) 1100Mjb/J (OT-I) mice were purchased from The Jackson Laboratory. Single spleen cells were suspended in 2 ml Red Blood Cell Lysis Buffer (Sigma-Aldrich) for 1 minute, washed, and resuspended at 2×10^6 cells/ml in RPMI culture medium containing 1 μg/ml OVA257-264 peptide, 5 μg/ml of mouse recombinant IL-2, and 40 μM 2-mercaptoethanol, and then incubated at 37°C for 5 days.

To set up the co-culture of OT-I and OVA^{+} tumor cells, splenocytes were harvested after 5-day activation. OT-I cells were purified using EasySep[TM] mouse CD8^{+} T Cell Isolation Kit (Stemcell technologies). Yumm5.2-OVA cells were seeded overnight. OT-I cells were then added into the culture at different time points. Cells were harvested by trypsinization and analyzed by flow cytometer.

BODIPY-C11 staining

Tumor cells (5000 cells/well) were seeded in 12-well plate and treated with IFNγ (10 ng/ml) or 40% T-cell supernatants, followed with arachidonic acid (AA). Then, cells were harvested by trypsinization for staining. For the co-culture of OVA^{+} tumor cells and OT-I cells, the mixture was collected and resuspended in 100 μl FACS buffer. Cells were first stained with anti-CD45 (30-F11) and anti-OVA257-264-H2Kb (25-D1.16) antibodies for 10 minutes at room temperature. To perform BODIPY-C11 staining, cells were resuspended in 1 mL Hanks Balanced Salt Solution (HBSS, Gibco 14-025-092), containing 5 μM BODIPY[TM] 581/591 C11 or BODIPY[TM] 665/676 and incubated for 15 minutes at 37°C in a tissue culture incubator. Cells were washed and resuspended in 200 μl fresh HBSS and analyzed immediately with a flow cytometer (LSR II, BD Biosciences). For BODIPY 581/591 C11 staining, the signals from both non-oxidized C11 (PE channel) and oxidized C11 (FITC channel) were monitored. The ratio of MFI of FITC to MFI of PE was calculated for each sample. The data were normalized to control samples as shown by relative lipid ROS.

Targeted phospholipid analysis

Acsl4^{+/+} and *Acsl4*^{-/-} Yumm5.2 cells were treated with IFNγ (10 ng/ml), arachidonic acid-d5 (10 μM) (Cayman Chemical), or both for 48 hours, collected by trypsinization, and washed with PBS. The cell pellet $(10^7$ cells) was re-suspended in 500 μl 25 mM HEPES (pH 7.4) containing 200 μM DTPA, and lysed by sonication on ice. Then, 500 μl methanol (high performance liquid chromatography, HPLC grade) was added. Samples were immediately frozen and kept at -80 °C. Upon thawing, after addition of an internal standard mix (EquiSplash; Avanti Polar Lipids), lipids were extracted using the Bligh & Dyer method. The organic phase was dried using a SpeedVac concentrator (Thermo Scientific) and resuspended in 100 μL of mobile phase A (hexanes/isopropanol 30:40 v/v) for injection into the liquid chromatography with tandem mass spectrometry (LC-MS/MS) system (Exion LC coupled to Triple Quadrupole 6500+, Sciex). Phospholipids were separated by class upon normal-phase HPLC using a gradient (25 %–95%) with mobile phase B (hexanes/isopropanol/water 30:40:7 v/v/v, 5 mM ammonium acetate) on a HILIC column (Kinetex 2.6 μm, 100 Å, 100 x2 .1 mm; Phenomenex). Ions were analyzed by multiple-reaction monitoring of phospholipid molecular species, containing d0- and d5-arachidonoyl chains in combination with common acyl chains: 16:0, 16:1, 18:0, 18:1, 18:2, 20:0, 20:2, 20:4, 20:5, 22:0, 22:2, 22:4, 22:5, and 22:6. The *m/z* transitions monitored were those from the deprotonated molecular negative ion (or the acetate adduct negative ion in the case of phosphatidylcholine species) to the corresponding acyl ion fragments. The chromatographic peaks (ion count *vs* time) for each analyte and internal standard were integrated using MultiQuant software (Sciex). Analyte relative abundances were calculated as the area ratio of each to the corresponding internal standard in their class.

Quantification of arachidonic acid

Tumor tissues were collected and placed in empty 15 ml conical tubes. Tissues were divided with scissors, wrapped with a 5-μm nylon filter paper (Sterlitech, WA), and stuffed (filter down) into a 1.5 ml conical tube. Tissues were centrifuged at 4,000 r.p.m. for 2 hours (Watson et al., 2021). Interstitial fluid and peripheral blood were used to detect arachidonic acid using an enzyme-linked immunosorbent assay, following the manufacturer's instructions (Biovision, CA, E4602).

Quantification of prostaglandin E2 (PGE2)

The interstitial fluid from tumor tissues were used to detect PGE2 using an enzyme-linked immunosorbent assay, following the manufacturer's instructions (Cayman, 500141).

Cell death measurement and immune profiling by FACS

For cell death analysis, cells were treated, collected, initially stained with specific antibodies, then resuspended in PBS containing 1 μg/ml Propidium Iodide (PI) or 7-Aminoactinomycin D (7-AAD) for 15 minutes, and directly run on a flow cytometer. For the co-culture of OVA⁺ tumor cells and OT-I cells, the mixture was collected and resuspended in 100 μl FACS buffer. Cells were first stained with anti-CD45 (30-F11) antibody for 10 minutes at room temperature, and then resuspended in FACS buffer containing 1 μg/ml PI for 10 minutes and analyzed by flow cytometry.

To quantify T cells and T cell cytokine expression, single-cell suspensions were prepared from fresh tumor tissues. T cells were enriched by density gradient centrifugation. For cytokine staining, T cells were incubated in culture medium containing PMA (5 ng/ml), Ionomycin (500 ng/ml), Brefeldin A (1: 1000), and Monensin (1: 1000) at 37°C for 4 hours. Anti-CD90 (53-2.1), anti-CD3 (17A2), anti-CD4 (RM4-5), and anti-CD8 (53-6.7) were added for 20 minutes for surface staining. The cells were then washed and resuspended in 1 ml of freshly prepared Fix/Perm solution (BD Biosciences) at 4°C overnight. After being washed with Perm/Wash buffer (BD Biosciences), the cells were stained with anti-TNF (MP6-XT22), anti-IFNγ (XMG1.2), and anti-granzyme B (16G6) for 30 minutes, washed, and fixed in 4% formaldehyde (Sigma Aldrich, 1004960700). All samples were read on an LSR II cytometer and analyzed with FACS DIVA software v. 8.0 (BD Biosciences).

Cell proliferation and viability assay

Tumor cells were harvested and seeded into 96-well plate. After adhesion, cells were treated with different ferroptosis inducers, inhibitors, or cisplatin. To determine the effect of treatment on cell growth and viability, 10% volume of alamarBlue (Bio-Rad, BUF012B) was directly added into medium and incubated for 4 - 6 hours. Absorbance at wavelengths of 570 nm and 600 nm was measured. The percent difference in reduction between treated and control cells was calculated using the following equation:

$$\text{Percent difference between treatment and control } (\%) = \frac{(117216 \times \text{A570 of treatment}) - (80586 \times \text{A600 of treatment})}{(117216 \times \text{A570 of control}) - (80586 \times \text{A600 of control})} \times 100$$

After calculation, the viability of control cells was 100% and all others were normalized to control and shown as relative cell number (%).

Quantitative PCR analysis

Total RNA was isolated from cells by column purification with Direct-zol RNA Miniprep Kit (R2053, Zymo Research) with DNase treatment. cDNA was synthesized using High-Capacity cDNA Reverse Transcription Kit (Thermo Fisher Scientific) with poly-dT or random hexamer primers. Quantitative PCR (qPCR) was performed on cDNA using Fast SYBR® Green Master Mix (4385618, Thermo Fisher Scientific) on a StepOnePlus™ Real-Time PCR System (Thermo Fisher Scientific). Gene expression was quantified using the following primers:

mouse Acsl4 forward: ATTGGTCAGGGGATATGGGCT;
mouse Acsl4 reverse: AGAGGAGCTCCAACTCTTCCA;
mouse Irf1 forward: TCCAAGTCCAGCCGAGACACTA;
mouse Irf1 reverse: ACTGCTGTGGTCATCAGGTAGG;
mouse Stat1 forward: GCCTCTCATTGTCACCGAAGAAC;
mouse Stat1 reverse: TGGCTGACGTTGGAGATCACCA;
mouse Actb forward: AGATCAAGATCATTGCTCCTCCT;
mouse Actb reverse: ACGCAGCTCAGTAACAGTCC;
mouse Gapdh forward: AGGAGAGTGTTTCCTCGTCC;
mouse Gapdh reverse: TGCCGTGAGTGGAGTCATAC;

Fold changes in mRNA expression were calculated by the ΔΔCt method using GAPDH or ACTB as an endogenous control. All fold changes are expressed normalized to the untreated control.

Immunoblotting

Cells were washed in cold PBS and lysed in 1× RIPA lysis buffer (Millipore, R0278) with 1× protease inhibitor cocktail (Roche, 11697498001). Lysates were incubated on ice for 10 minutes and cleared by centrifugation at 15,000 g for 15 minutes. Protein concentration was quantified using a BCA protein assay kit (Thermo Fisher, 23225). 30 μg total protein was mixed with sample buffer (Thermo Fisher, B0007) and denatured at 95°C for 10 minutes. Sample was separated by SDS-PAGE and transferred to a PVDF membrane (Millipore, IPVH00010). Membranes were blocked with 5% w/v nonfat dry milk and incubated with primary antibodies overnight at 4°C and HRP-conjugated secondary antibodies (Cell Signaling Technology (CST) Danvers, MA) for 2 hours at room

temperature. Signal was detected using Clarity and Clarity Max Western ECL Blotting Substrates (Bio-Rad) and captured using ChemiDoc Imaging System (Bio-Rad). Antibodies used were rabbit anti-ACSL4 (1:5000) (Abcam, ab155282), mouse anti-ACSL4 (1:1000) (Santa Cruz, sc-271800), anti-IRF1 (1:2000) (CST, 8478), anti-STAT1(1:1000) (CST, 9175), and anti-β-actin (1:5000) (CST, 5125).

Chromatin immunoprecipitation (ChIP)
ChIP assay was performed according to the SimpleChIP® Enzymatic Chromatin IP Kit (CST, 9003). In brief, Cells were fixed with formaldehyde and lysed, and chromatin was fragmented by partial digestion with Micrococcal Nuclease to obtain chromatin fragments of 1 to 5 nucleosomes. ChIP was performed using antibodies against IRF1 (CST, 8478) and IgG control (CST, 2729), and ChIP-Grade Protein G Magnetic Beads. After reversal of protein-DNA cross-links, the DNA was purified using DNA purification spin columns, ChIP-enriched chromatin was used for real-time PCR. Relative expression levels were normalized to input. Specific primers are listed in the Table S3.

In vitro T cell activation
Splenocytes (10^6/ml) from C57BL/6J mice were activated with anti-CD3 (eBioscience, 5 μg/ml) and anti-CD28 (eBioscience, 2.5 μg/ml) or other indicated concentration in the presence of 20 μM AA or tumor cell co-culture. The cells were subjected to surface marker and intracellular cytokine staining and analyzed by FACS. In a different setting, splenocytes from OT-I TCR transgenic mice were cultured with OVA loaded dead tumor cells for 3 days.

Mouse T cell isolation
Mouse T cells were isolated from spleen and lymph nodes in tumor-bearing mice. First, the cells are stained with a FITC-anti-mouse CD90 (53-2.1) primary antibody (BD Biosciences). Subsequently, the cells are magnetically labeled with Anti-FITC MicroBeads (Miltenyi Biotec). Then the cell suspension is loaded on a LS Columns (Miltenyi Biotec) which is placed in the magnetic field of a MACS Separator (Miltenyi Biotec). The magnetically labeled cells are retained in the column while the unlabeled cells run through. After removal of the column from the magnetic field, the magnetically retained T cells can be eluted as the positively selected cell fraction. The purity of T cells was more than 90% by FACS analysis.

QUANTIFICATION AND STATISTICAL ANALYSIS

No statistical methods were used to predetermine sample size. For cell-based experiments, biological triplicates were performed in each single experiment in general, unless otherwise stated. Animal experiments were performed in NSG and C57BL/6 mice. Animals were randomized into different groups after tumor cell inoculation; at least 5-9 mice were used for each group, unless otherwise indicated. Animals that failed to develop tumor were excluded from the analysis. Statistical analysis was performed using GraphPad Prism8 software (GraphPad Software, Inc.). Two tailed t-test and Mann-Whitney test were used to compare treatments vs. control groups. ANOVA models were used to compare continuous outcomes across multiple experimental groups, unless otherwise indicated in each figure legend. Survival functions were estimated by Kaplan-Meier methods and log-rank test was used to compare the survival distributions of difference groups.

Supplemental information

CD8^{+} T cells and fatty acids orchestrate

tumor ferroptosis and immunity via ACSL4

Peng Liao, Weimin Wang, Weichao Wang, Ilona Kryczek, Xiong Li, Yingjie Bian, Amanda Sell, Shuang Wei, Sara Grove, Jeffrey K. Johnson, Paul D. Kennedy, Miguel Gijón, Yatrik M. Shah, and Weiping Zou

Sub Class	Common Name	Synonyms	Molecular Formula	Yumm 5.2	B16F10	A375
Short-chain	Formic acid	C1:0	C1H2O1	1mM	1mM	1mM
	Acetic acid	C2:0	C2H4O2	1mM	1mM	1mM
	Propionic acid	C3:0	C3H6O2	1mM	1mM	1mM
	Butyric acid	C4:0	C4H8O2	1mM	1mM	1mM
	Isobutyric acid	C4:0	C4H8O2	1mM	1mM	1mM
	Valeric acid	C5:0	C5H10O2	1mM	1mM	1mM
Medium-chain	Caproic acid (Hexanoic acid)	C6:0	C6H12O2	100μM	100μM	100μM
	Caprylic acid (Octanoic acid)	C8:0	C8H16O2	100μM	100μM	100μM
	Capric acid (Decanoic acid)	C10:0	C10H20O2	100μM	100μM	100μM
	Lauric acid	C12:0	C12H24O2	40μM	100μM	100μM
Long-chain	Myristic acid	C14:0	C14H28O2	20μM	20μM	20μM
	Palmitic acid (PA)	C16:0	C16H32O2	20μM	20μM	20μM
	Stearic acid (SA)	C18:0	C18H36O2	20μM	20μM	20μM
	Arachidic acid	C20:0	C20H40O2	10μM	20μM	20μM
	Myristoleic acid	C14:1	C14H26O2	40μM	40μM	40μM
	Palmitoleic acid (POA)	C16:1	C16H30O2	40μM	40μM	40μM
	Oleic acid (OA)	C18:1	C18H34O2	40μM	40μM	40μM
	Linoleic acid (LA)	C18:2	C18H32O2	20μM	20μM	20μM
	Linoelaidic acid(γLA)	C18:2	C18H32O2	20μM	20μM	20μM
	α-Linolenic acid (αLA)	C18:3	C18H30O2	20μM	20μM	20μM
	Arachidonic acid (AA)	C20:4	C20H32O2	20μM	20μM	30μM
	Eicosapentaenoic acid (EPA)	C20:5	C20H30O2	20μM	20μM	20μM
Very long-chain	Behenic acid	22:0	C22H44O2	20μM	20μM	20μM
	Lignoceric acid	24:0	C24H48O2	10μM	10μM	10μM
	Erucic acid	22:1	C22H42O2	40μM	40μM	40μM
	Nervonic acid	24:1	C24H46O2	40μM	40μM	40μM
	Docosahexaenoic acid (DHA)	22:6	C22H32O2	20μM	20μM	

Table S1. All types of typical fatty acids that are used in this study, Related to Figure 1. The final concentrations of individual fatty acid applied to each cell lines are listed.
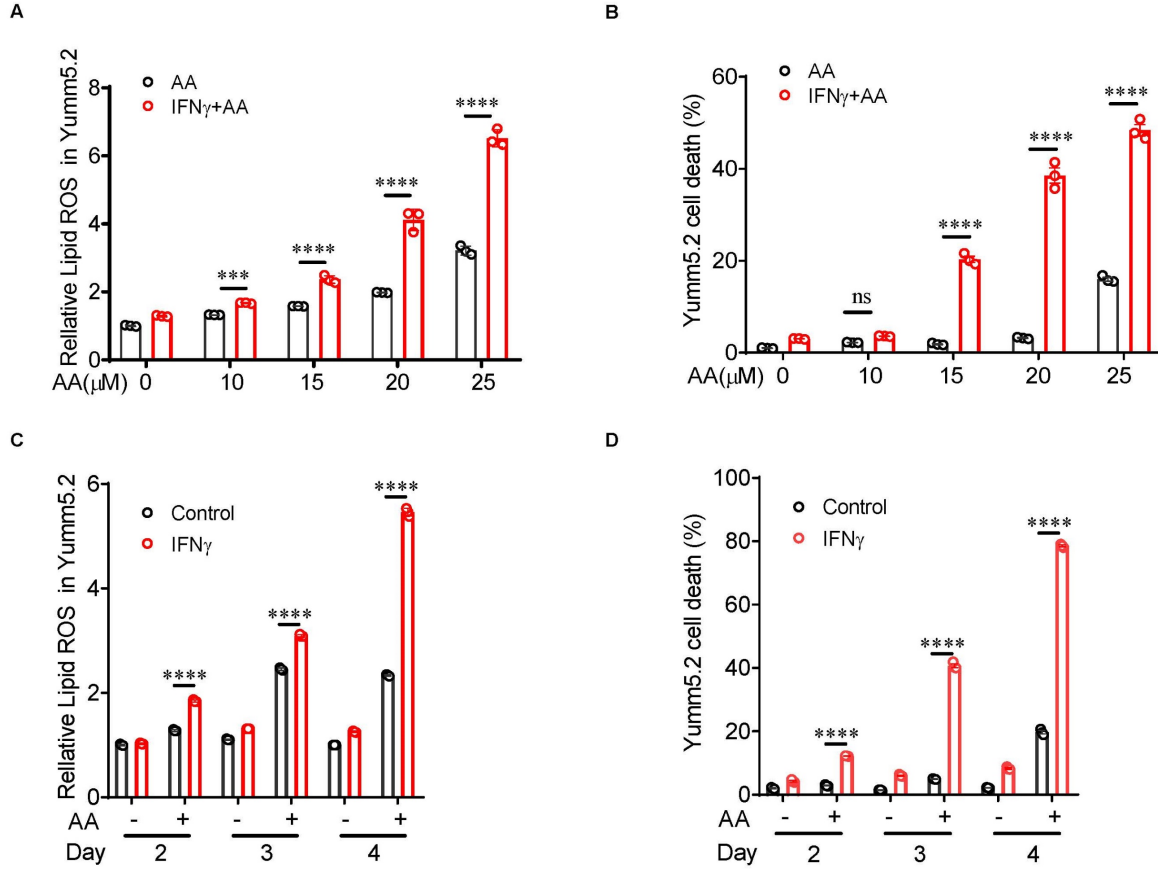
Figure S1. Effect of arachidonic acid and IFNγ on tumor cell death, Related to Figure 1.

(A and B) Percentage of relative lipid ROS (A) or dead cells (B) in Yumm5.2 cells treated with IFNγ plus different concentrations of arachidonic acid (AA) for 3 days. n = 3 biological replicates. ***P = 0.0003 and ****P < 0.0001 (A); ns, P = 0.64 and ****P < 0.0001 (B) (two-way ANOVA).

(C and D) Percentage of relative lipid ROS (C) or dead cells (D) in Yumm5.2 cells treated with IFNγ and AA for 2-4 days. n = 3 biological replicates. (two-way ANOVA). ****P < 0.0001 (C) and ****P < 0.0001 (D) (two-way ANOVA).
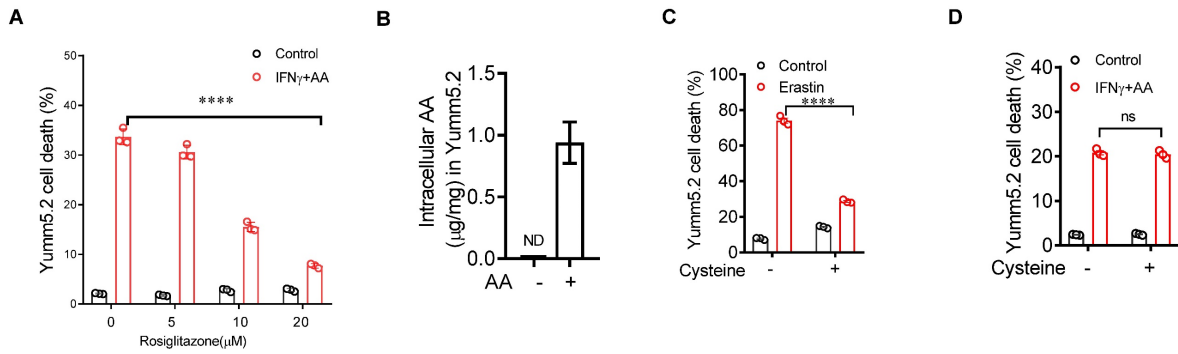
Figure S2. Effect of arachidonic acid and IFNγ on tumor ferroptosis, Related to Figure 2.

(A) Percentage of dead cells in Yumm5.2 cells treated with IFNγ plus AA for 3 days in the presence of different doses of Rosiglitazone. n = 3 biological replicates. ****P < 0.0001 (two-way ANOVA).

(B) AA levels in Acsl4$^{+/+}$ or Acsl4$^{-/-}$ Yumm5.2 cells treated AA (20 M) for 2 days. AA was detected by ELISA and normalized by tumor proteins. n = 2 biological replicates, ND, not detected.

(C) Percentage of dead Yumm5.2 cells treated with 2 M Erastin for 24 hours in the presence of 200 μM cysteine. n = 3 biological replicates. ****P < 0.0001 (two-way ANOVA).

(D) Percentage of dead Yumm5.2 cells treated with IFNγ and AA for 3 days in the presence of 200 μM cysteine. n = 3 biological replicates. ns, P = 0.98 (two-way ANOVA).
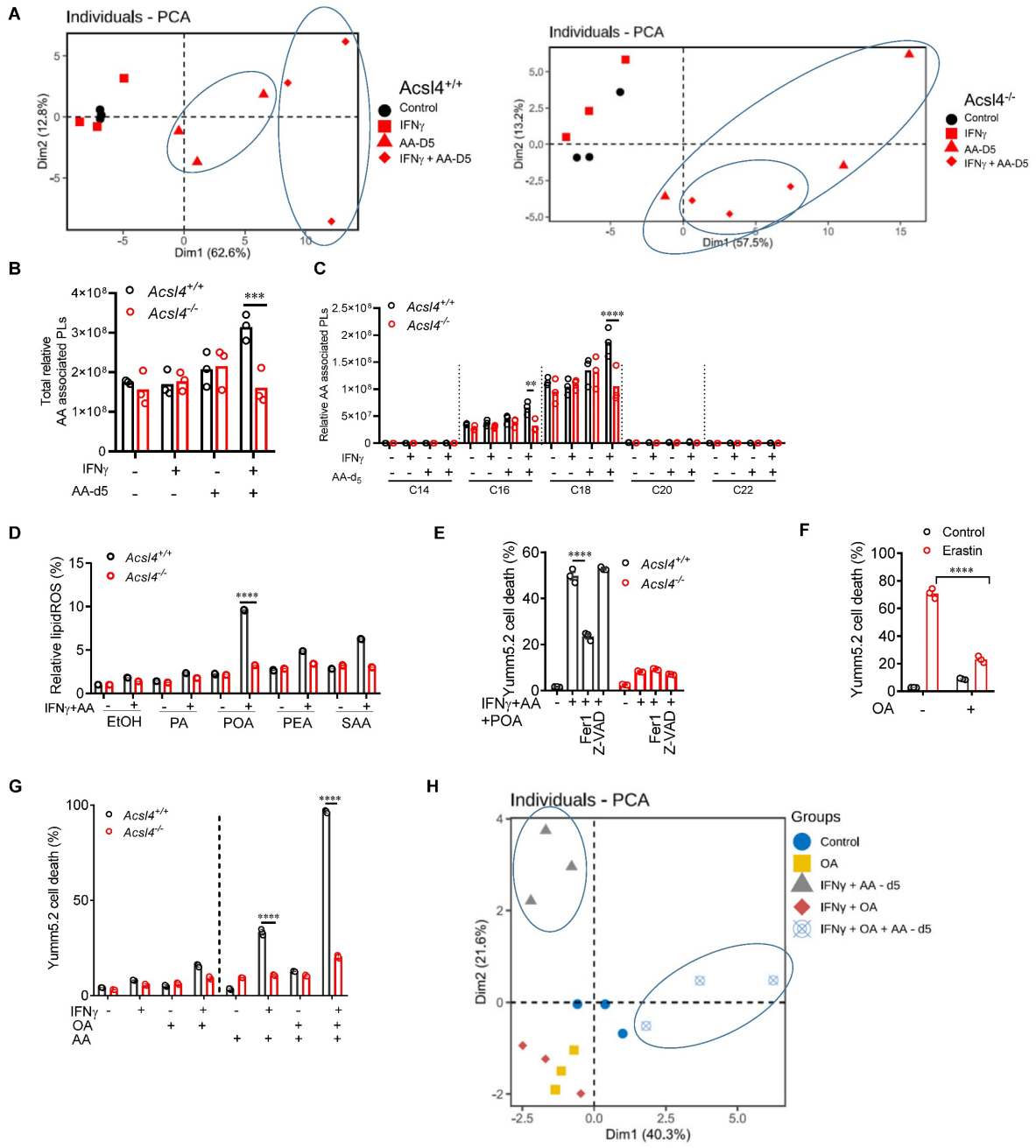
Figure S3. Role of IFNγ in ACSL4 associated phospholipids, Related to Figure 4.

(A) Principal component analysis (PCA) of lipid distribution in $Acsl4^{+/+}$ and $Acsl4^{-/-}$ Yumm5.2 cells. Yumm5.2 cells were treated with IFNγ, AA-d$_5$, and their combination for 48 hours. Lipids were analyzed by ultra-performance liquid chromatography–tandem mass spectrometry.

(B) Total AA (non-deuterated AA-d$_0$ and deuterated AA-d$_5$) associated phospholipids (PLs) in $Acsl4^{+/+}$ or $Acsl4^{-/-}$ Yumm5.2 cells treated with IFNγ, AA-d$_5$, and their combination for 48 hours. n = 3 biological replicates, mean ± s.d. ***$P = 0.0005$ (two-way ANOVA).

(C) Distribution of different length fatty acids in AA associated PLs in $Acsl4^{+/+}$ or $Acsl4^{-/-}$ Yumm5.2 cells treated with IFNγ, AA-d$_5$, and their combination for 48 hours. n = 3 biological replicates, mean ± s.d. *$P = 0.0407$, and ****$P < 0.0001$ (two-way ANOVA).

(D) Relative lipid ROS in $Acsl4^{+/+}$ or $Acsl4^{-/-}$ Yumm5.2 cells treated with IFNγ and AA (10 µM) in the presence of PA (20 µM), POA (60 µM), PEA (60 µM), and SAA (60 µM) for 48 hours. n = 3 biological replicates, mean ± s.d. ****$P < 0.0001$ (two-way ANOVA).

(E) Percentage of dead cells in $Acsl4^{+/+}$ or $Acsl4^{-/-}$ Yumm5.2 cells treated with IFNγ, AA (10 µM), and POA (40 µM) in the presence of ferrostatin-1 (2 µM Fer1) or z-VAD-FMK (10 µM z-VAD) for 48 hours. n = 3 biological replicates, mean ± s.d. ****$P < 0.0001$ (two-way ANOVA).

(F) Percentage of dead Yumm5.2 cells treated with Erastin in the presence of OA (60 µM) for 24 hours. n = 3 biological replicates (mean ± s.d.). ****$P < 0.0001$ (two-way ANOVA).

(G) Percentage of dead cells in $Acsl4^{+/+}$ or $Acsl4^{-/-}$ Yumm5.2 cells treated with IFNγ, OA (60 µM), AA (20 µM), and their combination for 3 days. n = 3 biological replicates, mean ± s.d. ****$P < 0.0001$ (two-way ANOVA).

(H) Principal component analysis (PCA) of lipid distribution in Yumm5.2 cells treated with I IFNγ, OA and AA-d5. Cells were treated with IFNγ (10 ng/ml), OA (60 µM), AA-d5 (10 µM) or their combinations for 48 hours Whole cell phospholipids were analyzed by ultra-performance liquid chromatography–tandem mass spectrometry. n = 3 replicates.

Sub Class	Common Name	Abbreviation	Synonyms	Systematic Name	Molecular Formula	Exact Mass
Saturate	Palmitic Acid	PA	C16:0	hexadecanoic acid	C16H32O2	256.2
	Stearic Acid	SA	C18:0	octadecanoic acid	C18H36O2	284.3
Unsaturate	Palmitoleic acid	POA	C16:1n-7	9Z-hexadecenoic acid	C16H30O2	254.2
	Palmitelaidic acid	PEA	C16:1n-7	9E-hexadecenoic acid	C16H30O2	254.2
	Sapienic acid	SAA	C16:1n-10	6Z-hexadecenoic acid	C16H30O2	254.2
	Oleic acid	OA	C18:1n-9	9Z-octadecenoic acid	C18H34O2	282.3
	Elaidic acid	EA	C18:1n-9	9E-octadecenoic acid	C18H34O2	282.3
	trans-vaccenic acid	VA	C18:1n-7	11E-octadecenoic acid	C18H34O2	282.3

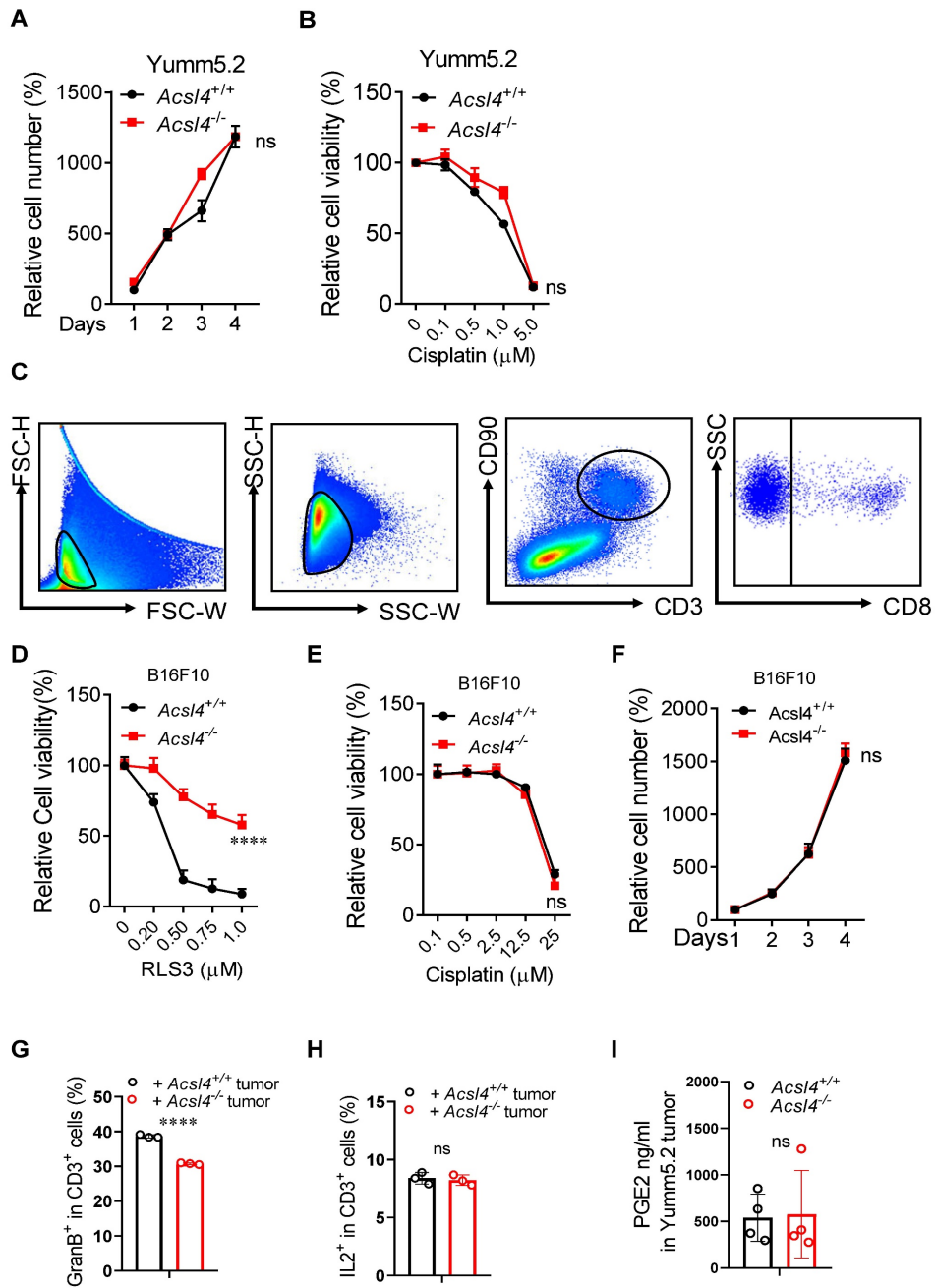Table S2. Isomers of C16:1 and C18:1 fatty acids. Related to Figure 4.

Figure S4. Role of tumor ACSL4 in tumor cells and T cells, Related to Figure 5.

(A) Relative cell numbers of $Acsl4^{+/+}$ or $Acsl4^{-/-}$ Yumm5.2 cells. Cell numbers were determined by alamarBlue assay on day 4. n = 4 biological replicates, mean ± s.d. ns, $P > 0.99$ (two-way ANOVA).

(B) $Acsl4^{+/+}$ or $Acsl4^{-/-}$ Yumm5.2 cell viability determined by alamarBlue assay. Tumor cells were treated with indicated concentrations of cisplatin for 24 hours. n = 4 biological replicates, mean ± s.d. ns, $P = 0.99$ (two-way ANOVA).

(C) Flow cytometry gating strategy showing T cell identification in the mouse tumor tissues.

(D - F) $Acsl4^{+/+}$ or $Acsl4^{-/-}$ B16F10 cells treated with different concentrations of RSL3 (D) or cisplatin (E) for 24 hours or cultured in complete medium for 1-4 days (F). Cell viability (D and E) and relative cell numbers (F) were determined by alamarBlue assay. n = 4 biological replicates. mean ± s.d. ****$P < 0.0001$ (D); ns, $P = 0.48$ (E) and ns, $P = 0.47$ (F) (two-way ANOVA).

(G and H) Percentages of granzyme B$^+$ (G) and IL-2$^+$ (H) in T cells co-cultured with $Acsl4^{+/+}$ or $Acsl4^{-/-}$ Yumm5.2 cells. ****$P < 0.0001$ (G); ns, $P = 0.69$ (H) (two-tailed t-test).

(I) PGE2 levels in $Acsl4^{+/+}$ or $Acsl4^{-/-}$ Yumm5.2 tumor tissues in tumor-bearing mice. PGE2 was measured by ELISA. n = 4 biological replicates. ns, $P = 0.89$ (two-tailed t-test).
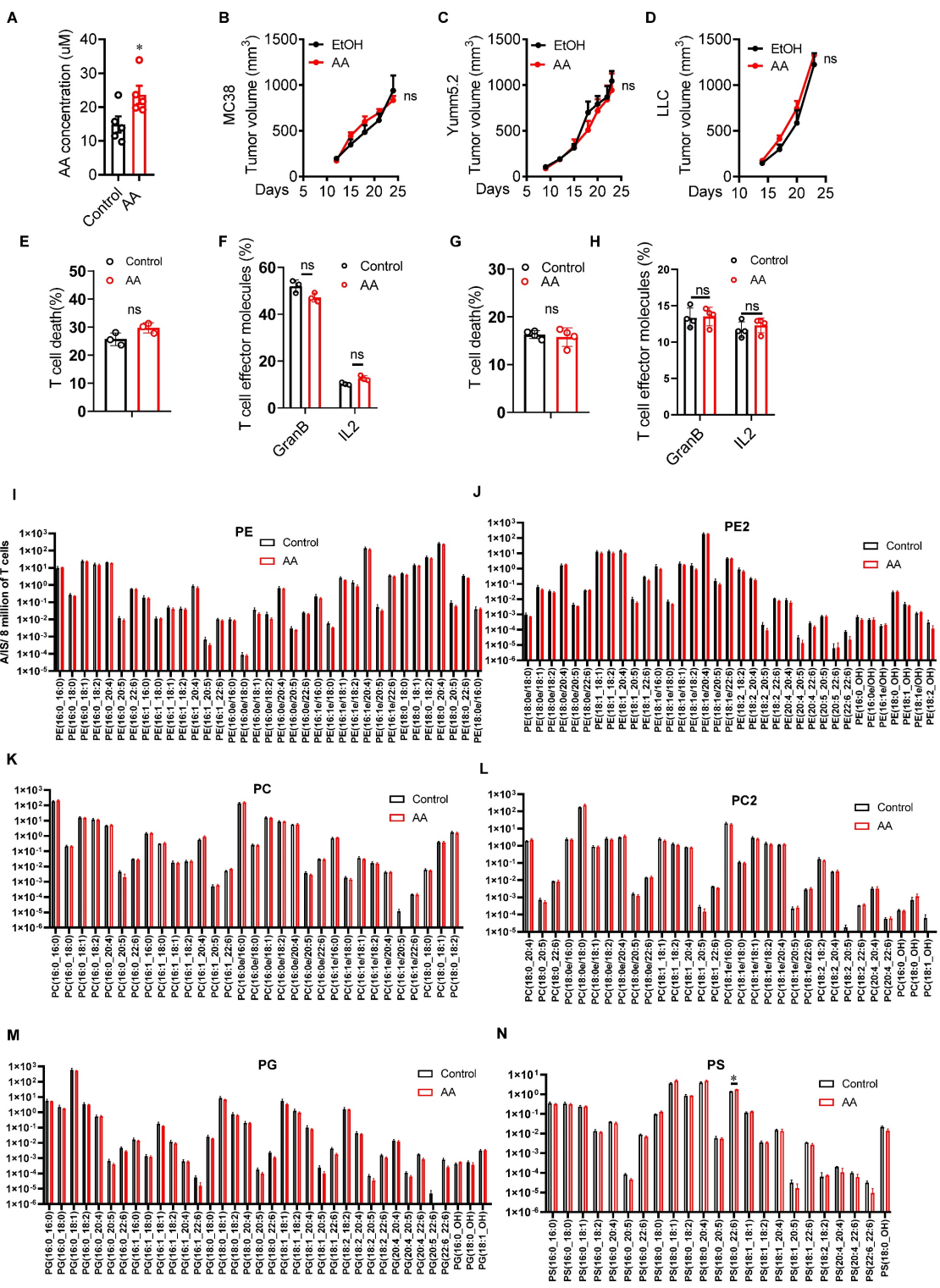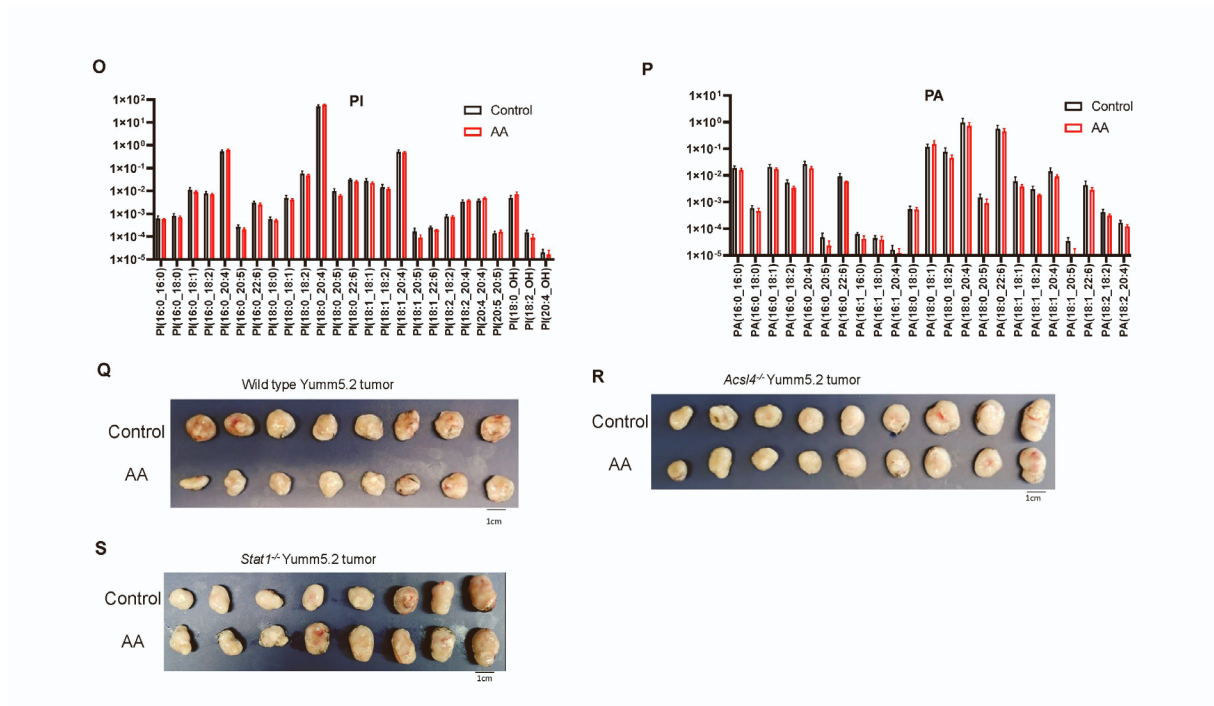
Figure S5. Impact of AA on T cells, Related to Figure 6.

(A) AA concentration in tumor tissue fluids. Yumm5.2 tumor-bearing mice were treated with PBS or AA. AA concentration was detected in tumor tissue fluids post one-day administration. *P = 0.0407 (two-tailed t-test).

(B-D) Effect of AA administration on tumor growth in NSG mice. NSG mice bearing MC38 (B), Yumm5.2 (C), and LLC (D) tumors were treated with PBS and AA. Tumor volume is shown. n = 3- 5 mice /group, mean ± s.e.m. ns, P = 0.85 (B), ns, P = 0.99 (C) and ns, P = 0.88 (D) (two-way ANOVA).

(E) Percentage of dead T cells. T cells were treated with AA (20 μM) for 72 hours *in vitro*. n = 3 biological replicates (mean ± s.d.). ns, P = 0.07 (two-tailed t-test).

(F) Percentages of granzyme B+ and IL-2+ T cells. T cells were treated with AA (20 μM) for 72 hours *in vitro*. ns, P = 0.13 and ns, P = 0.06; (Multiple t tests).

(G) Percentage of dead T cells in the tumor microenvironment. Yumm5.2 tumor-bearing mice were treated with AA (2 mg/kg). n = 4 biological replicates (mean ± s.d.). ns, P = 0.63 (two-tailed t-test).

(H) Percentages of granzyme B+ and IL-2+ T cells in the tumor microenvironment. Yumm5.2 tumor-bearing mice were treated with AA (2 mg/kg). ns, P = 0.97 and ns, P = 0.70 (Multiple t tests).

(I-P) Lipidomics profiling in T cells. Yumm5.2 tumor-bearing mice were treated with AA (2 mg/kg) as indicated. T cells were isolated and sorted for lipidomic profiling. Data are the mean values of the area of analyte (A) over the internal standard (IS) in 8×10^6 T cells. n = 4 biological replicates. log10-transformation has been applied to visualize and compare the abundance of the different phospholipid species in the samples. *P = 0.013; multiple t-test with Sidak–Bonferroni correction for multiple comparisons. Phosphatidylethanolamine (PE) (I and J), phosphatidylcholine (PC) (K and L), phosphatidylglycerol (PG)(M), phosphatidylserine (PS)(N), phosphatidylinositol (PI)(O) and phosphatidic acid (PA)(P).

(Q-S) Effect of AA administration on tumor growth *in vivo*. Wild type (Q), *Acsl4*$^{-/-}$ (R), and *Stat1*$^{-/-}$ (S) Yumm5.2 tumor-bearing mice were treated with PBS and AA. Tumor mass images are shown. n = 8-9 tumors/group.
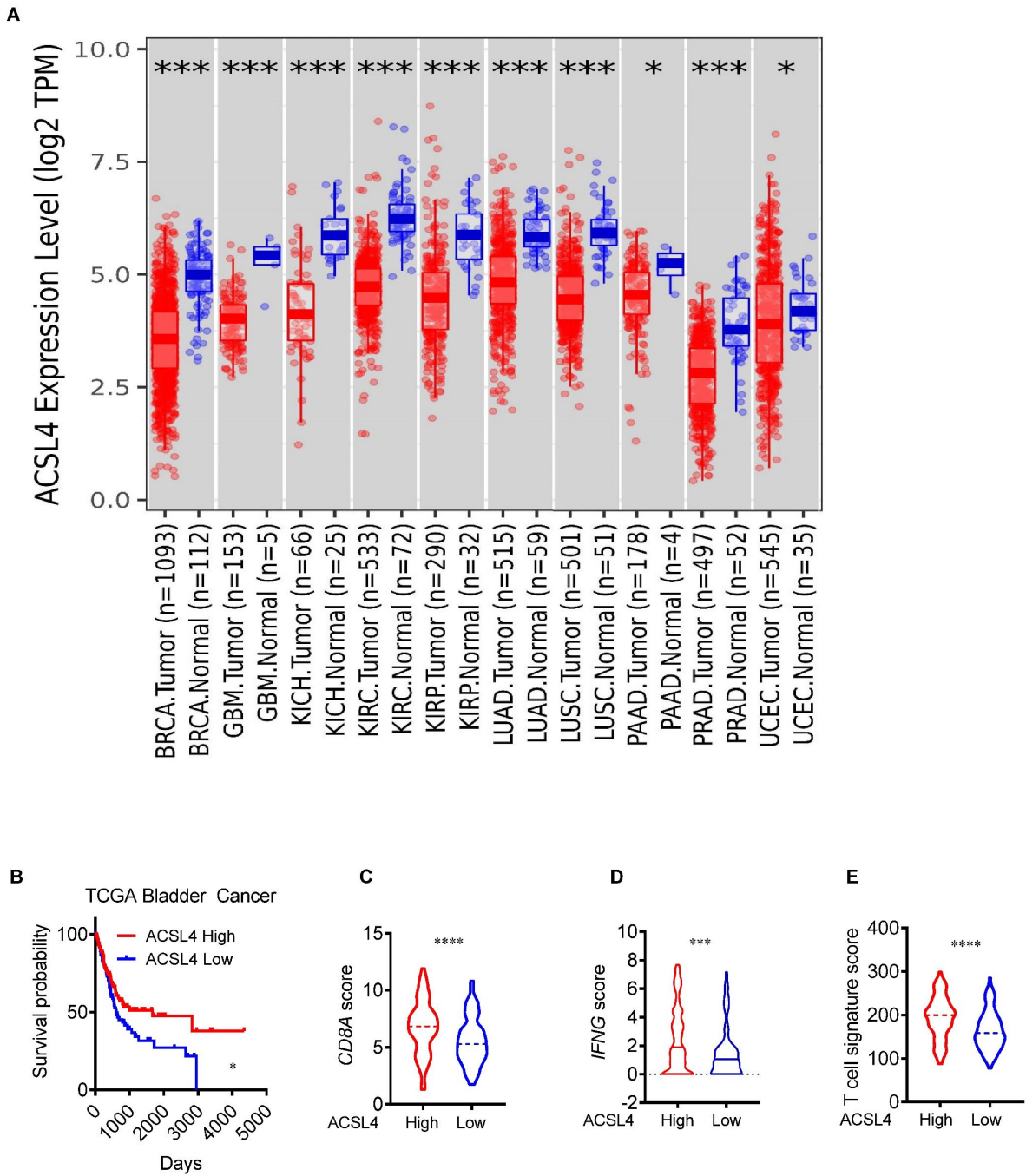
Figure S6. Clinical relevance of human tumor ACSL4, Related to Figure 6.

(A) ACSL4 expression in tumor and adjacent normal tissues in TCGA data sets. BRCA: Breast invasive carcinoma; GBM: Glioblastoma multiforme; KICH: Kidney Chromophobe; KIRC: Kidney renal clear cell carcinoma; KIRP: Kidney renal papillary cell carcinoma; LUAD:

Lung adenocarcinoma; LUSC: Lung squamous cell carcinoma; PAAD: Pancreatic adenocarcinoma; PRAD: Prostate adenocarcinoma; UCEC: Uterine Corpus Endometrial Carcinoma. The statistical significance computed by the Wilcoxon test is annotated by the number of stars (*P < 0.05; **P < 0.01; ***P < 0.001).

(B) Kaplan-Meier survival curves for bladder cancer patients with Low (bottom 25%) (n = 107) or High (top 25%) (n = 107) tumor ACSL4 transcripts in TCGA dataset. *P = 0.0489 (Log-rank test).

(C-E) Correlation between ACSL4 transcripts and immune genes - including CD8A of the minima, median, maxima and range for each blot are (1.28, 6.83, 11.92 and 10.64) (1.75, 5.29, 10.83 and 9.01) (C), IFNG of the minima, median, maxima and range for each blot are (0.0, 1.90, 7.68 and 7.68) (0.0, 1.05, 7.17 and 7.17) (D), and T cell signature score of the minima, median, maxima and range for each blot are (87.6, 199.7, 298.9 and 211.3) (77.5, 158.5, 285.6 and 208.1) (E) in TCGA dataset in patients with bladder cancer expressing High (n = 107) or Low (n = 107) levels of ACSL4. mean ± s.d. ****P < 0.0001 (C), ***P = 0.0009 (D) and ****P < 0.0001(E) (two-tailed t-test).

Binding Site (BS)	Primer Sequence
hACSL4-BS1	F:5'-CTCACTGCTGTTAGGCGCA-3'
	R:5'-CGATCCGCTTCTGTCAGTCTC-3'
hACSL4-BS2	F:5'-CAAAGCTGCGGTGACTTTTCC-3'
	R:5'-GTTAAGATCCCCGCTCACTCC-3'
hACSL4-BS3	F:5'-TGTAATCTCAGGTGGTAAGGCA-3'
	R:5'-TCCCTGATGCGTAATGGTGA-3'
hACSL4-BS4	F:5'-TCCGGGCGCGTCTTTTC-3'
	R:5'-AAGCTCGCAAAAAGGAACCG-3'
hACSL4-BS5	F:5'-CTCCGGGCGCGTCTTTTC-3'
	R:5'-AGCTCGCAAAAAGGAACCG-3'

Table S3. ChIP-qPCR primers for specific ACSL4 promotor region amplification, Related to STAR Methods.